Journal of Catalysis 450 (2025) 116277

Contents lists available at ScienceDirect

Journal of Catalysis

journal homepage: www.elsevier.com/locate/jcat

Research article

Catalytic activation of N_2O on promoted NiO based materials: Valorization by oxidative dehydrogenation of ethane

G. Sánchez-García [a], A. Pérez-Calvo [a], B. Moreno-Torralbo [b], R. Sánchez-Tovar [a], A.M. Dejoz [a], P. Concepción [b], J.M. López Nieto [b,*], B. Solsona [a,*]

[a] Departament áEnginyeria Química, Universitat de València, Av. Universitat s/n, 46100 Burjassot, Valencia, Spain
[b] Instituto de Tecnología Química, Universitat Politècnica de València-Consejo Superior de Investigaciones Científicas, Avenida de los Naranjos s/n, 46022 Valencia, Spain

ARTICLE INFO

Keywords:
N_2O
Oxidative dehydrogenation of ethane
Catalysis vs electrochemistry
Niobium
NiO
Temperature programmed reaction of ethane/N_2O

ABSTRACT

N_2O-assisted Oxidative Dehydrogenation (ODH) of ethane is an interesting way of simultaneously obtaining a highly valuable raw material (ethylene) and the functionalization of a greenhouse gas (N_2O). Unfortunately, over most of the catalytic systems, this reaction presents two main drawbacks: i) high yields to ethylene have hardly been reported; and ii) the catalytic activity highly decreases when replacing molecular oxygen by N_2O. In the present article, it will be shown that with promoted NiO catalysts, and using N_2O, high activity, comparable with that of conventional O_2-assisted ODH of ethane, is achieved. Furthermore, the use of the appropriate dopant, such as niobium, allows high ethylene yields (40 %), with a selectivity to ethylene of 72 % at 55 % ethane conversion. Overall, the catalytic results obtained indicate that the presence/absence and the nature of the promoter determines the catalytic performance of NiO based catalysts and the selectivity to ethylene can be explained on the basis of the electrochemical properties of the catalysts, correlating with parameters such as the density of acceptor defects (cationic vacancies) and the charge-transfer resistance at the interfacial active sites of the catalysts. Interestingly, the most selective catalyst (i.e., Nb-doped NiO) is highly robust as it presents stable catalytic performance after 24 h online and Ni^{2+} species are not reduced to Ni^0 even working at high temperatures in N_2O-free conditions.

1. Introduction

N_2O is a greenhouse gas present in the atmosphere with a relatively high concentration (~330 ppb), although behind CO_2 (~440 ppm) and methane (~1850 ppb). In particular, according to the latest data from the United States Environmental Protection Agency (EPA)[1], the contribution of N_2O to global warming has increased, and its emissions in 2021 represents 7 % of the global contribution of gases to the greenhouse effect. The long lifetime of nitrogen oxide in the atmosphere (over 114 years) has caused its global warming potential to be ca. 300 times greater than that of CO_2. In addition, in recent years both natural (agriculture) and, especially, anthropogenic emissions (production of nitric acid, adipic acid, burning of fossil fuels and biomass) have increased, so that the concentration in the atmosphere has increased since ~270 ppb in the pre-industrial era to 330 ppb today, 40 % of the emissions having a human origin [1–3]. 10 % of the overall emissions of N_2O proceeds from industry and wastewater treatment, the processes for nitric and adipic acid production being especially important. In the production of these acids, the emissions of N_2O can be decreased upgrading the technology to minimize N_2O formation, through the use of abatement equipment or by using N_2O as a reactant in useful reactions. In the present article, we have studied the last two approaches, especially the use of N_2O as an oxidant agent for the oxidative dehydrogenation of ethane.

Industrial processes which caused nitrous oxide emissions are directly related to petrochemical industry. In particular, almost 80 % of industrial N_2O emissions are generated as a by-product in adipic acid production [4]. N_2O is concentrated and released at the top of the nitric acid absorption tower in the adipic acid unit, while the tail gas generally contains significant amounts of N_2O, N_2, O_2, and CO_2, along with trace levels of NO and NO_2. To achieve high purity of N_2O from this tail gas, researchers have developed various processes, which typically involve absorption, adsorption, and distillation. The widespread use of these techniques in the separation and purification of gases, due to its

* Corresponding authors.
E-mail addresses: jmlopez@itq.upv.es (J.M. López Nieto), benjamin.solsona@uv.es (B. Solsona).

https://doi.org/10.1016/j.jcat.2025.116277
Received 10 February 2025; Received in revised form 26 May 2025; Accepted 7 June 2025
Available online 9 June 2025

simplicity and low energy requirements, will made possible the potential use of N_2O for industrial applications, such as the ethane ODH.

The use of N_2O as an oxidizing agent has gained renewed attention in the last years due, as mentioned before, to its negative impact on the global warming and its mild oxidizing character. The use of N_2O for the oxidative dehydrogenation of ethane has been reported previously [5–12]. Unfortunately, apart from ethylene, other undesired reaction products, mainly CO and CO_2, are usually obtained. The most studied catalysts are those based on vanadium oxides [6–8]. Vanadium supported on siliceous MCM41 material reached a selectivity to ethylene of 55–60 % at 8 % conversion (at 500 °C) using N_2O as an oxidant agent [6]. Although these results are not outstanding, a massive improvement was observed compared to the analogous experiments using O_2, that, at that conversion, the selectivity to ethylene hardly exceeded 10 %. The best performance using nitrous oxide was reported to be due to the absence of unselective non-lattice oxygen species which can be formed from O_2 but not from N_2O [8].

Other materials have been also tested in the N_2O-ODH of ethane. Supported molybdenum catalysts can selectively activate ethane in the presence of N_2O but it requires high reaction temperatures (ca. 600 °C) and the conversions attained are low [9,10]. In addition, the activation energy of re-oxidation when using N_2O is 98 kJ mol^{-1}, whereas that of O_2 is 41 kJ mol^{-1} leading to a re-oxidation rate at least 1700 times faster when O_2 is the oxidant [9]. In that article, temperature-programmed oxidation of the pre-reduced (after TPR) catalysts was undertaken with O_2 or N_2O. The oxidant consumption presented a maximum, which was different depending on the oxidizing agent. Then, in the case of O_2, the maximum consumption took place at 265 °C whereas in the case of N_2O the maximum was at 481 °C. This experiment confirms that oxygen is a stronger oxidizing agent than nitrous oxide [9].

On the other hand, iron sites if properly distributed can also activate both N_2O and ethane at lower temperatures than molybdenum (ca. 400 °C). As iron on ZSM-5 catalysts have been reported to be able to activate N_2O for the selective oxidation of benzene into phenol [11] it was proposed that these materials could be also efficient for the N_2O mediated ODH of ethane. Positively, iron modified on several zeolites (ZSM-5, mordenite, faujasite) selectively activate ethane in the N_2O-ODH in contrast with Fe impregnated on silica or amorphous silica–alumina [12]. It was highlighted the importance of the net charge of the matrix in the formation of selective iron species. Interestingly, iron complexes accommodated in ZSM-5 channels showed the highest activity, in which N_2O oxidant was partly utilized for ethane oxidation (towards ethylene or carbon oxides), while some part of the oxidant was decomposed to nitrogen and oxygen.

When comparing the exchange of oxygen in the surface of NiO single crystals with $N^{18}O$, $^{18}O_2$ and $N_2^{18}O$ [13], it was observed that N_2O exchanges its oxygen even more slowly than molecular oxygen and tends to decompose before the oxygen exchanges.

Currently, apart from multicomponent Mo-V-Te-Nb-O mixed oxide catalysts [14–18], the most efficient materials for the ODH of ethane using O_2 as an oxidant agent are based on nickel oxide [19–32]. Although pure NiO presents very low selectivity to ethylene during the ODH of ethane [33], and can be slightly improved by optimizing the synthesis method [34], the best catalytic results are observed when NiO is supported [19–23] or modified by promoters [24–32]. In this way, it has been observed that when the cation added has a higher valence (Al^{3+}, Ga^{3+}, Ti^{4+}, Sn^{4+}, Nb^{5+}, Ta^{5+} or W^{6+}) the positive p+ hole concentration decreases and a removal of unselective high oxidation state nickel oxide take place [24–32]. In this way, a correlation between the valence of the dopant cation and the selectivity to ethylene has been established [24,29]. In addition, the presence of electrophilic O^- species seems to be necessary for the activation of ethane [30], although its concentration must be low in order to prevent oxidation to carbon oxides (CO and CO_2) [35].

On the other hand, materials based on NiO have been also reported to be capable to decompose N_2O at relatively low reaction temperatures [36–41]. Overall, NiO is among pure metal oxides one of the materials that gets the highest N_2O decomposition rate [36] and this performance was associated to the low heat of formation of the nickel oxide. Then, unstable oxides seem to enhance the reactivity of the active sites. The performance of NiO can be further improved using bismuth doped NiO catalysts, this enhanced activity being related to the presence of high concentrations of both Ni^{3+} and surface oxygen vacancies on NiO [37]. The addition of other dopants such as Ba and Ce to NiO ($Ce_{1.0}Ba_{1.5}Ni_9Ox$ catalyst) led to an important synergistic effect, Ce facilitating the N_2O dissociation and Ba improving the O_2 desorption [38].

Then, the catalysts to efficiently carry out the N_2O-assisted ethane ODH require presence of catalytic sites that both decompose N_2O and activate ethane selectively. In both cases, the promotion with other elements of NiO have meant an enhanced catalytic performance. In this way, Ni-Al mixed oxides derived from layered double hydroxides [42], sulfate-modified NiAl mixed oxides [43] and NiO—CeO_2—ZrO_2 [44] catalysts have been tested in the N_2O-ODH of ethane, demonstrating an excellent performance, better than that of a simple supported NiO/Al_2O_3 catalyst [42]. The best performance of the Ni-Al mixed oxide was attributed to the presence of isolated O^- species and a weak adsorption of the olefin that avoids its overoxidation. On the other hand, mesoporous Ni—Fe—Al_2O_3 catalysts have been also studied for this reaction, [45] those samples with highly dispersed Ni^{2+}-species and iron oxide species with close proximity, showing the best catalytic performance. In any case, the yields to ethylene obtained did not exceed 20 %. Table S1 shows a summary of representative results reported in the literature.

In addition, it has been suggested that an increase in the proportion of isolated electrophilic oxygen species may also favour greater ethylene selectivity [43,46]. In this case, the isolated oxygen species would favour an effective rupture of the C—H bonds (with easy desorption of the olefinic intermediate), while the presence of adjacent oxygen species hinders the desorption of the olefinic intermediate, favouring the formation of the combustion product.

Surprisingly, a systematic study for the N_2O-assisted ethane ODH over promoted NiO catalysts, including the representative Nb-promoted NiO catalyst, has not been undertaken at present, being this the goal of this study.

In the present article, a comprehensive electrochemical characterization of the catalysts has been conducted to explore the electron transfer processes driving the redox reactions involved in ethane ODH assisted by N_2O. Therefore, a deep study of NiO catalysts doped with different promoters has been done using the Electrochemical Impedance Spectroscopy (EIS) technique in order to determine the resistance values of the active layers of the catalysts, the capacitance analysis of the space charge layer (Mott-Schottky) to check the type and extent of the semiconductor behaviour and the cyclic voltammetry to measure the electrochemical activity. Additionally, the aim is to further elucidate the role of nucleophilic oxygen species and their correlation with ethylene selectivity.

This work will cover two important aspects; on one hand, the study of different doped NiO catalysts for the N_2O assisted ODH of ethane; and, on the other hand, a deep electrochemical study of doped NiO samples. Thus, it has been established a correlation between the selectivity to ethylene in the N_2O assisted ODH of ethane and the electrochemical properties of the catalysts.

2. Experimental

2.1. Catalyst preparation

Promoted NiO catalysts (with a promoter/Ni at. ratio of 1/9) were synthesized through the evaporation at 80–90 °C of aqueous solutions of nickel nitrate ($Ni(NO_3)_2$ $6H_2O$, Sigma-Aldrich) and the corresponding metal salt of the promoter. Moreover, oxalic acid ($C_2H_2O_4$, Sigma-Aldrich) was added with a Ni/oxalic acid molar ratio of 1. The synthesis was undertaken in a 250 mL beaker using 50 mL of deionised water

and the corresponding salts. These mixtures were continuously stirred and evaporated in ca. 5 h. The paste obtained was dried overnight at 120 °C in a furnace and then calcined at 500 °C in static air for 2 h (10 °C/min temperature ramp). The promoter/Ni and the oxalic acid/Ni ratios have been selected as they are in the range of the optimal values as reported in the O_2-ODH of ethane [29].

Several cations have been considered as promoters in this study (i.e., Bi^{3+}, Fe^{3+}, In^{3+}, Ce^{3+}, Ti^{4+} and Nb^{5+}) and the corresponding catalysts were named as (Bi)NiO, (Fe)NiO, (In)NiO, (Ce)NiO, (Ti)NiO and (Nb)NiO, respectively. In this way, several salts have been employed: bismuth(III) nitrate pentahydrate ($Bi(NO_3)_3{\cdot}5H_2O$, Sigma-Aldrich); iron (III) nitrate nonahydrate ($Fe(NO_3)_3{\cdot}9H_2O$, Sigma-Aldrich), indium(III) nitrate hydrate ($In(NO_3)_3{\cdot}xH_2O$, Sigma-Aldrich), cerium(III) nitrate hexahydrate ($Ce(NO_3)_3{\cdot}6H_2O$, Sigma-Aldrich), titanium butoxide ($C_{16}H_{36}O_4Ti$, Sigma-Aldrich) and ammonium niobate(V) oxalate hydrate ($C_4H_4NNbO_9{\cdot}xH_2O$, Sigma-Aldrich).

Two different unpromoted nickel oxide catalysts have been prepared. In one case, using the same procedure than in the promoted catalyst but without the addition of the promoter salt, including the oxalic acid addition. This catalyst has been named as **NiO-I**. The second catalyst, named as $\mathbf{NiO_{ref}}$, has been synthesized just evaporating a nickel nitrate aqueous solution, drying in furnace and a further calcination in static air at 500 °C for 2 h.

2.2. Characterization techniques

The specific surface areas were estimated by the Brunauer- Emmet-Teller (BET) method from N_2 adsorption isotherms at 77 K (− 196 °C) measured in a Micromeritics TriStar 3000 instrument. 200 mg (0.25–0.40 mm) of catalyst, was initially degassed under vacuum at 250 °C/2 h.

X-ray diffraction patterns were recorded with a PANalytical CUBIX instrument equipped with a graphite monochromator, by using Cu Ka radiation (k = 0.1542 mm) and operating at 45 kV and 4 mA. Data were acquired over a 2θ range of 10 − 90° with the scan rate of 1° min^{-1} and a step size of 0.02°.

Temperature-programmed reduction experiments (TPR-H_2) were carried out in an Autochem 2910 (Micromeritics) equipped with a TCD detector. The reducing gas composition was 10 % H_2 in Ar (total flow rate of 50 mL min^{-1}), and using a heating rate of 10 °C min^{-1} until 800 °C. In all cases, 50 mg of catalyst, in pellets (0.25–0.40 mm), was used.

X-ray photoelectron spectra were collected using a SPECS spectrometer with an MCD-9 detector and a non-monochromatic AlKα (1486.6 eV) X-Ray source. Spectra were recorded using a pass energy of the analyser at 50 eV, an X-ray power of 100 W and under an operating pressure of 10^{-9} mbar. During data processing of the XPS spectra, binding energy (BE) values were referenced to C1s peak (284.5 eV), and the spectra treatment has been performed using the CasaXPS software.

IR-CO were done at −170 °C using a Nexus 8700 FTIR spectrometer equipped with a DTGS detector and acquiring at 4 cm^{-1} resolution. Experiments were done employing a home-made IR cell connected to a vacuum system with gas dosing facility for in situ treatments in controlled atmospheres and temperatures. For IR studies, the samples (~13 mg) were pressed into self-supported wafers and treated at 200 °C in oxygen flow (20 ml min^{-1}, using a heating rate of 10 °C min^{-1}) for 2 h followed by evacuation at 150 °C, 10^{-4} mbar, for 1.5 h. After activation, the samples were cooled down under dynamic vacuum conditions to −176 °C followed by CO dosing at increasing pressure (0.05–2 mbar). The cooling time from 150 °C to −176 °C was ~45 min. IR spectra were recorded after each dosage. Spectra devolution has been done using the ORIGIN software.

TPR-N_2O experiments were conducted using a quartz micro reactor coupled to a quadrupole mass spectrometer (MS, Omnistar, Balzers). 80 mg (0.25–0.40 mm) catalyst diluted in 320 mg CSi was pre-activated in 20 vol% O_2 flow (18 mL min^{-1}) at 400 °C, 1 h with a heating rate of 10 °C min^{-1}. After pre-activation the sample was cooled down in O_2 flow (18 mL min^{-1}) to 25 °C. The cooling time from 400 °C to 25 °C was ~45–60 min. Once stabilized the temperature; the reactant feed was switched to 1 vol% N_2O/He flow 25 mL min^{-1}. Reaction temperature was increased up to 500 °C with a heating ramp of 10 °C min^{-1} and the reaction products analyzed by on line MS.

TPR-N_2O/Ethane experiments were conducted using the same set up as before and similar reaction conditions but, instead of ramping up the temperature in a flow of 1 vol% N_2O/He, a mixture of 5 vol% Ethane and 10 vol% N_2O was used. The mass fragments used in the MS files are: m/z = 28 (N_2); m/z = 44 (N_2O); m/z = 18 (H_2O); m/z = 32 (O_2).

Electrochemical interfacial properties of the catalysts were studied in a three-electrode electrochemical cell with an Ag/AgCl 3 M KCl reference electrode and a platinum wire as counter electrode. The catalysts were connected to the potentiostat as working electrodes with 0.5 cm^2 of exposed area to the electrolyte.

Electrochemical Impedance Spectroscopy (EIS) tests, Mott-Schottky (MS) measurements and cyclic voltammetries were carried out to characterize the catalysts, specifically their electrochemical properties at the interface between the catalysts (electrodes) and the electrolyte. Electrochemical Impedance Spectroscopy (EIS) is based on perturbing an electrochemical system at equilibrium or in a steady state by applying a sinusoidal signal (AC voltage or AC current) over a wide frequency range and monitoring the corresponding sinusoidal response (current or voltage, respectively). Mott-Schottky analysis involves measuring the space charge capacitance at the semiconductor interface as a function of potential, according to Eq. (1):

$$\frac{1}{C^2} \approx \frac{1}{{C_H}^2} - \frac{1}{{C_{SC}}^2} = \frac{1}{{C_H}^2} - \frac{2}{e{\cdot}\varepsilon_T{\cdot}\varepsilon_0{\cdot}N_A}{\cdot}\left(E - E_{FB} - \frac{k{\cdot}T}{e}\right) \quad (1)$$

where C_{SC} is the space charge layer capacitance, C_H is the Helmholtz layer capacitance, e the electron charge ($1.60{\cdot}10^{-19}$ C), ε_0 the vacuum permittivity ($8.85{\cdot}10^{-14}$ F/cm), ε the relative dielectric constant of the semiconductor, N_A acceptor defects corresponding to the cationic vacancies, E the applied potential, k the Boltzmann constant ($1.38{\cdot}10^{-23}$ J/K) and T the absolute temperature. Cyclic voltammetry measurements were recorded to investigate the electrochemical activity of the different catalysts.

Before EIS measurements, catalysts were immersed in the solution for 1800 s at 0.5 VAg/AgCl. After this pre-treatment, EIS tests were carried out applying a potential of 0.5 VAg/AgCl using an amplitude of 0.01 V and scanning frequencies from 100 kHz to 0.01 Hz. Mott-Schottky plots were performed at a frequency of 5000 Hz, scanning the potential from 1 to −0.5 VAg/AgCl at 0.05 V/s using an amplitude signal of 0.01 V. Cyclic voltammetries were performed in the potential range of −0.1 to 0.6 VAg/AgCl at 0.01 V/s. The electrolyte used for MS and EIS tests was 0.1 M of $Na_2(SO)_4$, while for the cyclic voltammetries, a solution of 10 mM of $Fe(CN)_6^{-}$ K_4 with 0.1 M Na_2SO_4 was employed.

2.3. Catalytic tests

N_2O assisted Oxidative Dehydrogenation (ODH) of ethane tests were conducted in a fixed-bed quartz reactor, at atmospheric pressure, in the range of 300–425 °C, mainly at 400 °C. The reactor was heated in a conventional tubular metallic oven. For the control of the temperature, a thermocouple was employed. The thermocouple was located in a sheath at mid height of the catalytic bed. The gradient of the temperature observed along the catalytic bed was never higher than 1 °C. Silicon carbide was used in the catalytic bed together with the catalyst to minimize hot spots. The feed consisted of an ethane/N_2O/He mixture with a 5/10/85 M ratio. Although the ratio of the reactants was kept constant, different experiments were carried out changing the total flow and/or the catalyst mass (total flow between 25 and 100 mL min^{-1} and amount of catalyst between 0.05 and 0.5 g of catalyst) in order to achieve several contact times and consequently, different conversions. Two

analyses in each conditions were conducted using a stabilization period of 45 min. Reactants and reaction products were analysed by gas chromatography using two packed columns: (i) molecular sieve 5A (MS, 2.5 m); and (ii) Porapak Q (PQ, 3 m). About the cromatographic method, the following cycle (with a valve to change the columns working) was used: 0–1.5 min PQ + MS (after that period hydrogen, oxygen, nitrogen and CO entered the MS column). 1.5–10 min PQ (in this period CO_2, N_2O, ethane, ethylene and water exit). 10–20 min PQ + MS (in this period H_2, N_2, O_2 and CO exit). 20–45 min PQ (just in case other hydrocarbons or acids, such as acetic acid, are formed). We must also mention that water was not condensed as the lines are heated after the reactor until the loop of the GC.

For comparison, some experiments were also undertaken using molecular oxygen as an oxidizing agent. In that case, for a proper comparison, the number of O-atoms was maintained the same as in the N_2O experiments. Then, the feed consisted of an ethane/O_2/He mixture with a 5/5/90 M ratio.

3. Results

3.1. Physico-chemical characterization of catalysts

Some representative physicochemical characteristics of the synthesized catalysts are shown in Table 1. The nature of the promoters has been selected considering that alkali or earth alkali promoters have a deleterious effect in the ODH of ethane using O_2 as an oxidizing agent [29]. Therefore, the oxidation state of the promoters in the oxide formed when calcined in static air has been established in 3+ or higher.

The surface area of the unpromoted catalysts is the lowest (for both cases lower than 20 $m^2\ g^{-1}$), especially in the case of the sample prepared in the absence of oxalic acid (10.7 vs 18.5 $m^2\ g^{-1}$ for samples prepared without or with oxalic acid, respectively). This means that the addition of oxalic acid has some positive effect for enhancing the surface area, since an increase of ca. 75 % takes place compared to the **NiO_{ref}** catalyst. On the other hand, neither pure NiO catalysts nor doped catalysts present microporosity in agreement with other authors [19–26].

The inclusion of a promoter led to an increase of the surface area until 40–70 $m^2\ g^{-1}$, depending on the metal. It means that the addition of a heteroatom has led to the formation of smaller nanoparticles. Those samples with Bi^{3+} and Fe^{3+} present the lowest surface area (40–45 $m^2\ g^{-1}$) whereas those with Ce^{4+}, Ti^{4+} and Nb^{5+} have the highest values (64–68 $m^2\ g^{-1}$).

The XRD patterns of unpromoted and promoted NiO catalysts are shown in Fig. 1A. In all cases, the main phase corresponds to the face-centred cubic NiO phase (JCPDS 47–1049). The mean crystallite size of cubic NiO phase was the highest for the undoped reference sample (ca. 25 nm). The simple addition of oxalic acid during the preparation procedure led to a decrease in the crystallite size until ca. 18 nm, in agreement with the increase observed in the surface area. The doping with different elements meant a further decrease in the crystallite size, until 9.7–12.1 nm, depending on the nature of the promoter. For the undoped catalysts or those doped with Fe or Nb, NiO has been the only crystalline phase detected. However, in the case of the catalysts doped with bismuth, indium, cerium or titanium, low intensity peaks of Bi_2O_3 (JCPDS: 78–1793), In_2O_3 (JCPDS: 06–0416), CeO_2 (JCPDS: 34–0394) and anatase TiO_2 (JCPDS: 21–1272) have been detected, respectively.

Table 1
Physicochemical characteristics of the nickel oxide-based catalysts synthesized.

Catalyst[a]	S_{BET} ($m^2\ g^{-1}$)	H_2-TPR T_{max} (°C)[b]	H_2-TPR T_{onset} (°C)[b]	NiO Crystal size (nm)[c]
NiO-I	18.5	305 (329, 358)	241	17.8
(Bi)NiO	41.3	313	242	11.8
(Fe)NiO	44.6	(313) 359	265	12.1
(Ce)NiO	66.7	337	260	9.7
(Nb)NiO	64.6	373	260	10.5
(In)NiO	55.5	397	250	9.8
(Ti)NiO	67.5	424	291	9.8
NiO_{ref}	10.7	(290) 386	261	24.8

[a] Promoted NiO catalysts (with a promoter/Ni at. ratio of 1/9).
[b] Temperature of the maximum reduction (T_{max}) and temperature of onset (T_{onset}) during the TPR-H_2 experiments; in parenthesis, reduction temperatures for other shoulders.
[c] Mean crystallite size determined by XRD using the Scherrer equation considering the peaks at 2θ = 37 and 43° of NiO (JCPDS: 47–1049).

As the ethane oxydehydrogenation mainly takes place on the nickel oxide-based catalysts through a redox mechanism [19–30], the study of the reducibility of these samples could provide us useful information. Temperature Programmed Reduction (TPR) profiles of the nickel oxide-based catalysts (Fig. 1B) shows maxima that vary from 305 to 424 °C depending on the sample. The reference NiO catalyst presents a maximum at 386 °C with a low intensity shoulder at ca. 300 °C. The use of oxalic acid led to an increase in the reducibility, shifting the maximum until 305 °C, with two more shoulders at 329 and 358 °C. These bands have been assigned to the reduction of bulk NiO. It has been proposed that NiO of different nature, including non-stoichiometric nickel oxide or NiO with distinct crystallite size, present different reducibility and consequently different shoulders are visible [34,36]. In this case, the lower reducibility of the NiO_{ref} catalyst must be due to the higher crystallite size, that makes difficult the Ni^{2+} to Ni^0 transition.

The addition of the different promoters meant an important change in the TPR profiles compared to the NiO-I catalysts [47]. Thus, the addition of bismuth or cerium slightly changed the reduction profile, whereas the addition of iron, niobium and, especially, titanium displaced the reduction bands towards higher temperatures. The shift of the bands can be linked to the interaction between NiO particles and the promoters, either incorporated to the lattice or the promoter oxide crystallites. Unfortunately, it has not been possible to relate the different shifts with the valence of the promoter, the cation radius, the formation of the crystallites of the oxide of the promoter or the surface Ni species (qv. post by XPS).

The surface properties of nickel sites in unpromoted and promoted catalysts are studied by X-ray photoelectron spectroscopy (XPS). The Ni $2p_{3/2}$ core line of the different catalysts is shown in Fig. 2 and their values summarised in Table S2, whereas the Ni 2p core level spectra of catalysts are shown in Fig. S1. As shown in Fig. 2, in all samples, three components at around 853.5, 855.7 and 860.5 ± 0.3 eV are observed at the Ni $2p_{3/2}$ core line, which according to the literature has been referred as the main peak (853.3 ± 0.3 eV) and satellite peaks at 855.4 ± 0.3 eV (Satellite I) and 859.9 ± 0.3 eV (Satellite II) [48].

The signal at 855.4 eV has been associated to Ni^{2+}—OH species [49], Ni^{2+} vacancies [50], or as a result of non-local screening mechanism [51]. Interestingly, the intensity of the former peak at 855.4 eV versus the main peak is similar in all samples, except in the (Nb)NiO, where it is slightly higher (see Table S2). This may be related to different local environment of nickel sites and is in line with the different electrochemical properties of the sample compared to the others, as will be shown later.

In this way, the different environment of Ni sites is confirmed by IR − CO employing CO as a probe molecule to determine the chemical state of metal sites [52]. According to the IR spectra displayed in Fig. 3, Lewis sites of higher acid character are observed in the case of the (Nb)NiO and (Ce)NiO samples, characterised by IR bands at 2191 and 2179 cm^{-1} for the (Nb)NiO sample and at 2161 cm^{-1} for the(Ce)NiO one, compared to that of the un-doped ones located at 2156–2153 cm^{-1}. In order to avoid the involvement of dipole–dipole effects which shift the IR bands, undermining accurate discussion of Lewis acid sites, the herein IR spectra corresponds to low CO dosing (in Fig. S2 the IR at increasing CO coverage). Thus, assuming that a higher positive CO frequency shift, ν (C≡O)), corresponds to a higher Me-CO binding energy which can be related to a higher Lewis acidity [52,53], the following trend in the acid nature of Ni Lewis sites can be given: (Nb)NiO > (Ce)NiO > NiO-I =

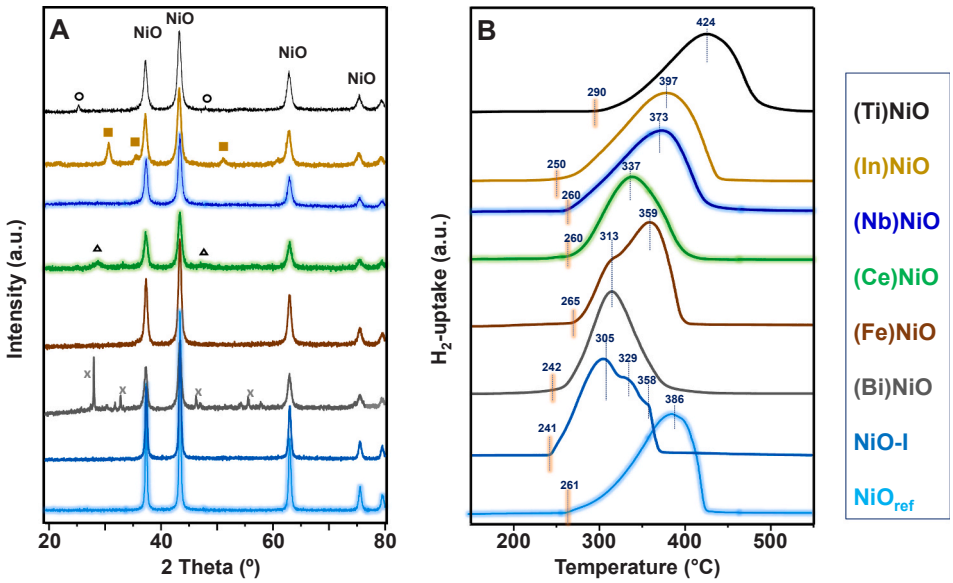

Fig. 1. XRD patterns (**A**) and Temperature Programmed Reduction, H_2-TPR, profiles (**B**) of unpromoted and promoted nickel oxide catalysts. In the H_2-TPR profiles, it has been also included T_{max} (see also Table 1). In Fig. 1A other crystalline phases apart from NiO have been also detected: Bi_2O_3 (x), CeO_2 (Δ), In_2O_3 (■) and anatase TiO_2 (o).

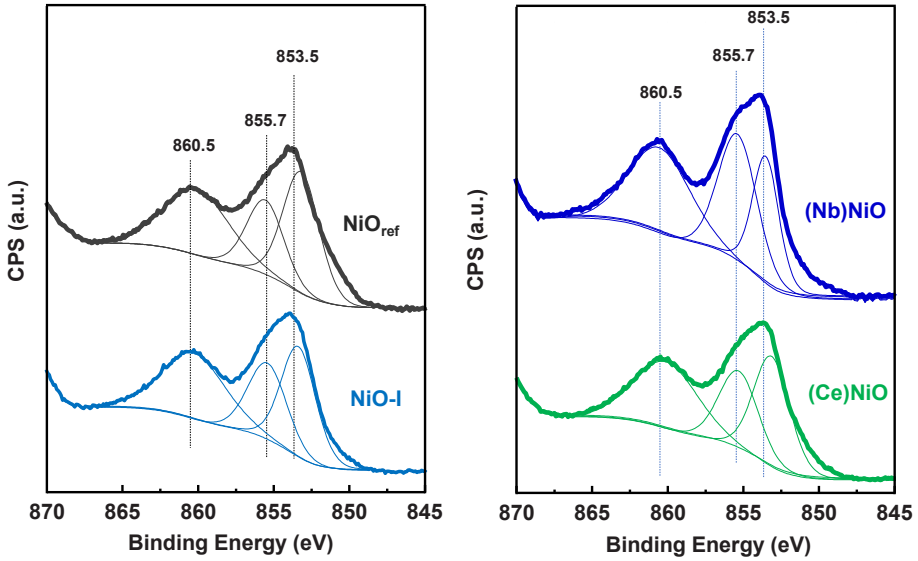

Fig. 2. Ni $2p_{3/2}$ core line of undoped and doped NiO catalysts.

NiO_{ref}, underlying a key role of the promoter on the nature of Ni species. This is in good agreement to previous results for ethane ODH using oxygen as an oxidant [29], in which the nature of surface sites seems to be strongly influenced by the valence and the acid/base characteristics of the metal oxide promoters, which have a great impact on the selectivity to ethylene [29].

3.2. Catalytic results

The main carbon containing reaction products identified in the N_2O assisted ethane ODH have been ethylene and CO_2. Interestingly, no CO was detected. This absence of CO must be related to the high reactivity of these catalysts for the CO oxidation to CO_2 [35]. In this way, Table S3 shows the catalytic results for CO oxidation to CO_2 for two representative catalysts; i.e., **NiO-I** and (Nb)NiO catalysts. Interestingly, for both cases, the CO conversion exceeds 99 % at only 250 °C.

Pure NiO as well as Me-promoted NiO (Me= Nb, Bi, Fe, In, Ce, Ti and Bi) catalysts have been tested in the N_2O assisted ethane ODH. As shown in Table 2 the **NiO_{ref}** catalyst presents the worse catalytic performance since, in the reaction conditions tested, the alkane conversion achieved is the lowest as well as the selectivity to ethylene.

This negative performance is more notorious considering that the selectivity to ethylene decreases with the conversion of ethane. Just by preparing the **NiO-I** catalyst, in the presence of an adequate amount of oxalic acid, the selectivity to ethylene highly increases. An improvement compared to the **NiO_{ref}** catalyst is also obtained by all the promoted catalysts. We must note that promoted catalysts have been also synthesized with the same oxalic acid amount than that of **NiO-I** catalyst. If working at isoconversion conditions (i.e., at 30 % ethane conversion), the difference in selectivity to ethylene is even more notorious between the **NiO_{ref}** catalyst and the other catalysts.

According to the results obtained, the gravimetric rate (per mass of

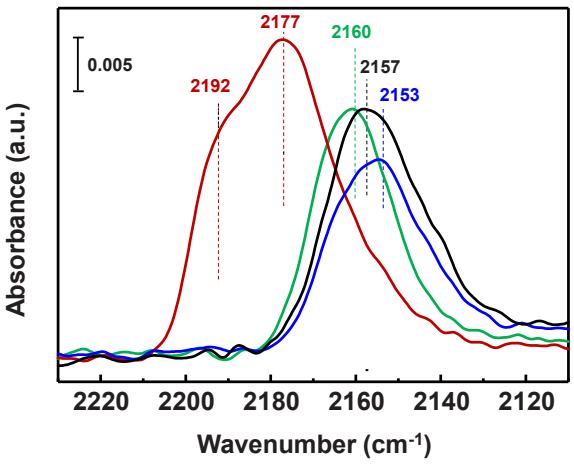

Fig. 3. IR spectra of CO adsorption at 0.3 mbar and −176 °C on (Nb)NiO (red), (Ce) NiO (Green), NiO-I (blue) and NiO_{ref} (black) samples. (For interpretation of the references to colour in this figure legend, the reader is referred to the web version of this article.)

catalyst) of the **NiO_{ref}** catalyst increases when either oxalic acid is used in the preparation of catalysts or when promoters are added. The addition of oxalic acid in the preparation of pure NiO catalysts during the preparation method means a drastic increase in the activity of ca. 185 %. Similarly, when nickel oxide is doped the increase in the gravimetric rate is lower, as it varies between 50 (in the case of Fe^{3+}) and 180 % (in the case of Nb^{5+} and Ce^{4+}), depending on the nature of the promoter. Therefore, it seems that the addition of promoters diminishes the activity compared to **NiO-I** and this decrease depends on the nature of the dopant.

The enhanced activity of the active sites of the oxalic acid treated **NiO-I** catalyst is more evident if the surface area of the catalysts is considered. Then, the specific activity per m^2 of the **NiO-I** catalyst is 3–5 times that of the promoted catalysts (Table 2), the **NiO_{ref}** catalyst presenting an intermediate specific activity.

For unpromoted NiO catalysts, the use of oxalic acid during synthesis resulted in a moderate increase in surface area but a significant increase in gravimetric rate. Consequently, the activity per surface area is still much higher for the NiO-I catalyst. Therefore, the dramatic increase in catalytic activity is due to the increased surface area and, especially, to the greater intrinsic reactivity of the active sites. On the other hand, the use of promoters tends to considerably increase the surface area but entails a decrease in gravimetric rate. This means that the activity per surface area decreases considerably compared to the unpromoted NiO catalyst synthesized with oxalic acid. It is therefore plausible that the addition of promoters eliminates some of the active sites. Fig. 4A presents the variation of the selectivity to ethylene with the ethane conversion at 400 °C for some representative catalysts. In all cases, a moderate decrease in the selectivity to ethylene has been observed when increasing the ethane conversion. Most (Ti- and Nb-doped) and least (pure and Bi-doped) selective catalysts behave like this at both low and high ethane conversions. Using these non-optimized reaction conditions, a yield to ethylene of ca. 40 % has been achieved with the Nb-doped NiO catalyst.

On the other hand, for a proper comparison of the selectivity to ethylene we have to consider the same ethane conversion and the same reaction temperature. Then, Fig. 4B shows that comparison at 30 % ethane conversion and 400 °C. It can be seen that all the other catalysts are far better than the reference **NiO_{ref}** catalyst. Between pure NiO and the best catalyst (Nb-doped NiO) there is ca. 40 points difference in ethylene selectivity.

The order of selectivity to ethylene observed is: **NiO_{ref}** < (Bi)NiO < **NiO-I**, (Fe)NiO, (In)NiO < (Ce)NiO < (Ti)NiO < (Nb)NiO. Thus, the improvement in the selectivity is not observed in all cases when compared to the optimized promoter free NiO catalyst. The addition of bismuth means a decrease of the olefin formation whereas the inclusion of Ce^{4+} and, especially, Ti^{4+} and Nb^{5+}, leads to an increase in the ethylene formation. Promoters such as Fe^{3+} and In^{3+} do not seem to exert any important effect.

All the former experiments have been undertaken using an ethane to N_2O molar ratio of 0.5 (ethane 5 %, N_2O 10 %). Table S4 (supplementary information) shows experiments undertaken with the same concentration of alkane and the same amount of catalyst and total flow but modifying the N_2O concentration (increasing or decreasing the amount of inert gas). Then, it can be seen that the ethane conversion increases and the selectivity to ethylene decreases when the N_2O concentration increases. In these conditions, the maximum yield to the olefin was obtained using a 10 % N_2O in the fed (Table S3). Low concentrations of N_2O diminished the activity whereas high concentrations decreased the selectivity to the olefin. A comparative study between ODH of ethane with O_2 or with N_2O was also conducted on (Nb)NiO catalyst (Table S5). Meanwhile the catalytic activity hardly changes using N_2O as an oxidizing agent compared to molecular oxygen, at isoconversion conditions the selectivity to ethylene significantly increases 8–10 % (Fig. S3A).

Another parameter that should be studied to check the robustness of these catalysts is their stability with the time on line. Thus, the N_2O assisted ODH of ethane requires the catalysts to be able to activate both N_2O and ethane. Thus, activating the N_2O molecule, we should observe both carbon oxides (during ethane deep oxidation) and water (during both ODH and deep oxidation of ethane). The amount of N_2O required for the oxidative transformation of ethane to ethylene is determined

Table 2
Oxidative dehydrogenation of ethane using N_2O as an oxidant agent on NiO based catalysts.[a]

Catalyst	Ethane Conversion (%)[b]	Selectivity C_2H_4 (%)[b]	Selectivity CO_2 (%)[b]	Ethylene yield (%)[b]	Gravimetric Rate (X < 15 %)[c,d]	Specific Activity (X < 15 %)[c,e]	Selectivity to Ethylene (at X = 30 %)[f]
NiO-I	51.1 ± 0.2	51.8	48.2	26.5	24.4	13.2	60
(Ce)NiO	51.0 ± 0.5	57.0	43.0	29.1	27.8	4.16	64
(Bi)NiO	37.7 ± 0.1	50.9	49.8	19.2	14.6	3.88	52
(Fe)NiO	27.0 ± 0.1	61.7	38.3	16.7	11.0	2.46	59
(In)NiO	34.9 ± 0.3	58.3	41.7	20.3	14.3	2.57	60
(Ti)NiO	49.2 ± 0.2	67.8	32.2	33.4	24.4	3.62	71
(Nb)NiO	50.2 ± 0.1	72.6	27.4	36.5	24.5	3.79	80
NiO_{ref}	18.1 ± 0.1	44.0	56.0	10.1	5.49	5.13	37

[a] $C_2/N_2O/He$: 5/10/85 M ratio, Reaction temperature = 400 °C.
[b] m_{cat} = 0.2 g; Total flow = 50 mL min^{-1}.
[c] determined at 400 °C for ethane conversions lower than 15 %.
[d] activity per mass of catalyst in 10^{-3} mol_{C2H6} g_{cat}^{-1} h^{-1}.
[e] in 10^{-4} mol_{C2H6} m^{-2} h^{-1}.
[f] Selectivity to C_2H_4 (%) at ethane isoconversion of 30 % determined at 400 °C (variable contact time).

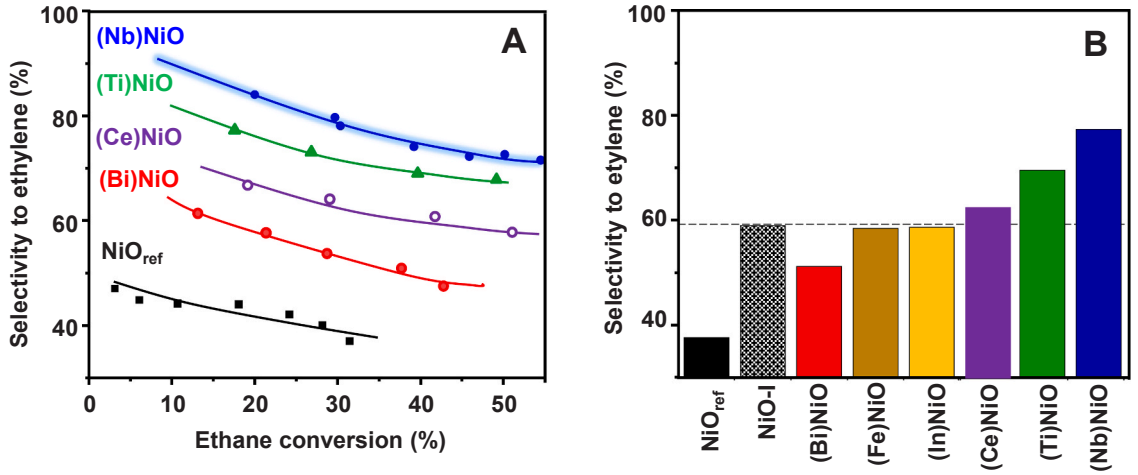

Fig. 4. A) Variation of the selectivity to ethylene with the ethane conversion for representative NiO based catalysts at 400 °C: **B)** Selectivity to ethylene in the N_2O-assisted ODH of ethane at 400 °C, and at isoconversion conditions (30 % ethane conversion), for undoped and doped NiO catalysts. Symbols: NiO_{ref} (■); NiO-I (□); (Bi)NiO (●); (Ce)NiO (○); (Ti)NiO (▲); and (Nb)NiO (●). Remaining reaction conditions in text. For comparative purposes, a dashed line in Fig. 4B corresponding to the value of the selectivity of the unpromoted NiO catalyst prepared similarly to the promoted samples, is included.

according to the following equation:

$$C_2H_6 + N_2O \rightarrow C_2H_4 + H_2O + N_2$$

This means that for the formation of 1 molecule of ethylene, 1 molecule of N_2O is required. In these experiments, we have observed only two C-containing reaction products, ethylene and CO_2. In the case of the formation of carbon dioxide, the consumption of N_2O per molecule of ethane reacted is much higher:

$$C_2H_6 + 7\ N_2O \rightarrow 2\ CO_2 + 3\ H_2O + 7\ N_2$$

Then, for the transformation of 1 molecule of ethane to CO_2, 7 molecules of N_2O are required. Considering this stoichiometry, we can estimate the N_2O conversion required by knowing the ethane conversion and the selectivity to the reaction products. For almost all cases, the N_2O conversion measured fits very well with the theoretical one, according to the formation of ethylene and CO_2. An example of this is shown in Supporting Information.

Fig. 5 shows a stability study undertaken for three representative catalysts (i.e., **NiO_{ref}**, (Ce)NiO and (Nb)NiO catalysts) at 400 °C. In the case of pure **NiO_{ref}** catalyst (Fig. 5A), we studied the catalytic stability of this catalyst maintaining the same conditions for 7 h and monitoring the activity and selectivity. Interestingly, a stable performance was observed without apparent variations in the ethane conversion or selectivity to ethylene and the N_2O conversion measured fitted very well with the theoretical one. Accordingly, no appreciable differences were observed in the XRD pattern after and before the use. For both cases, the only crystalline phase observed was cubic NiO (JCPDS: 47–1049) with the main peaks at 2θ of ca. 37, 43 and 63°, maintaining a similar mean crystallite size (24.8 nm for the fresh catalyst and 24.5 nm for the used one).

In the case of the most selective catalyst (i.e., (Nb)NiO sample) (Fig. 5B) a further catalytic test in the N_2O-ODH reaction was undertaken at 400 °C for 7 h confirming a very stable performance. Accordingly, the XRD patterns did not show appreciable differences for both fresh and used catalysts, just with a subtle increase of the average size of the NiO phase nanodomains (10.5 nm for the fresh and 11.0 nm for the used sample). The surface area of the used catalyst was also very similar to that of the fresh catalyst (64.6 vs 62.7 m^2/g). For comparison, the study of the (Ti)NiO catalyst is also presented in Fig. S3B.

Conversely, the catalyst with cerium, (Ce)NiO, presented a completely different behaviour (Fig. 5C). In the first analysis, the ethane conversion was ca. 50 % and the selectivity to ethylene was 55–60 %, ethylene and CO_2 being the only C-containing products detected. Interestingly, in this case, the N_2O conversion measured (ca. 84 %) was lower than that required for the formation of the reaction products (ca. 92 %). This means that the oxygen atoms from the reaction products have proceeded not only from the N_2O fed but also from the lattice of the catalyst. However, in accordance with this observation, after 2.5 h on line the catalytic performance drastically varied. Thus, the ethane conversion raised from ca. 50 % to ca. 90 % whereas the selectivity to ethylene decreased from ca. 55 % to 0 %. In these conditions, the C-containing reaction products identified were CO, CO_2 and CH_4. Hydrogen was also detected as a result of the ethane reforming reaction that also produces COx. A XRD analysis of the fresh catalyst showed the presence of cubic NiO as a majority and CeO_2 (JCPDS: 43–1002) as a minority. However, the pattern of the catalyst after use had changed in a way that the predominant phase was metallic Ni phase (JCPDS: 4–0850) with main diffraction peaks at ca. 44 and ca. 52°. NiO and CeO_2 were also detected as minorities. This reduction of the nickel oxide to metallic nickel confirmed the exhaustion of the lattice oxygen, which was necessary to carry out the reaction.

In contrast with the (Nb)NiO catalyst, the (Ce)NiO catalyst drastically changed its structure after the use in Fig. 5, forming metallic nickel. This reduced catalyst was re-calcined at 500 °C/2 h and the surface area measured. Unfortunately, an important decrease of the surface area was observed in the (Ce)NiO catalyst (from 66.7 to 36.1 m^2/g).

Therefore, the nature of the promoter has an influence on the relative ethane and N_2O activation. Thus, Nb^{5+} is a better promoter than Ce^{4+}, since leads to higher formation of ethylene, which is less O-consumer than CO_2. Then, at similar ethane conversion (50 %) the Nb-doped catalyst does not consume all the N_2O whereas that with Ce consumes more O-atoms than those of the N_2O fed. Thus, the Nb-doped catalyst has a balanced capacity for activating ethane and N_2O to achieve stability, whereas the Ce-doped catalyst seems to have preference when increasing the reaction temperature for the N_2O activation and the consequent CO_2 formation, this way creating an oxygen poor atmosphere not capable to develop a stable behaviour. To the best of our knowledge, the catalytic results presented in this article are among the best reported up to date in the N_2O-assisted ODH of ethane (Table S1), with stable yields to ethylene of ca. 40 %. Only, sulphated NiAlO catalysts [43] present similar yields but at reaction temperatures much higher than those of the present article (600 °C vs 400 °C).

3.3. Electrochemical properties of doped NiO catalysts

Additionally, a deep electrochemical study, including electrochemical impedance spectroscopy and the evaluation of the semiconducting properties using Mott-Schottky plots, has been also conducted on these catalysts in order to try to establish a relationship with their catalytic properties. Interestingly, clear correlations between electrochemical and catalytic parameters have been detected. EIS is a

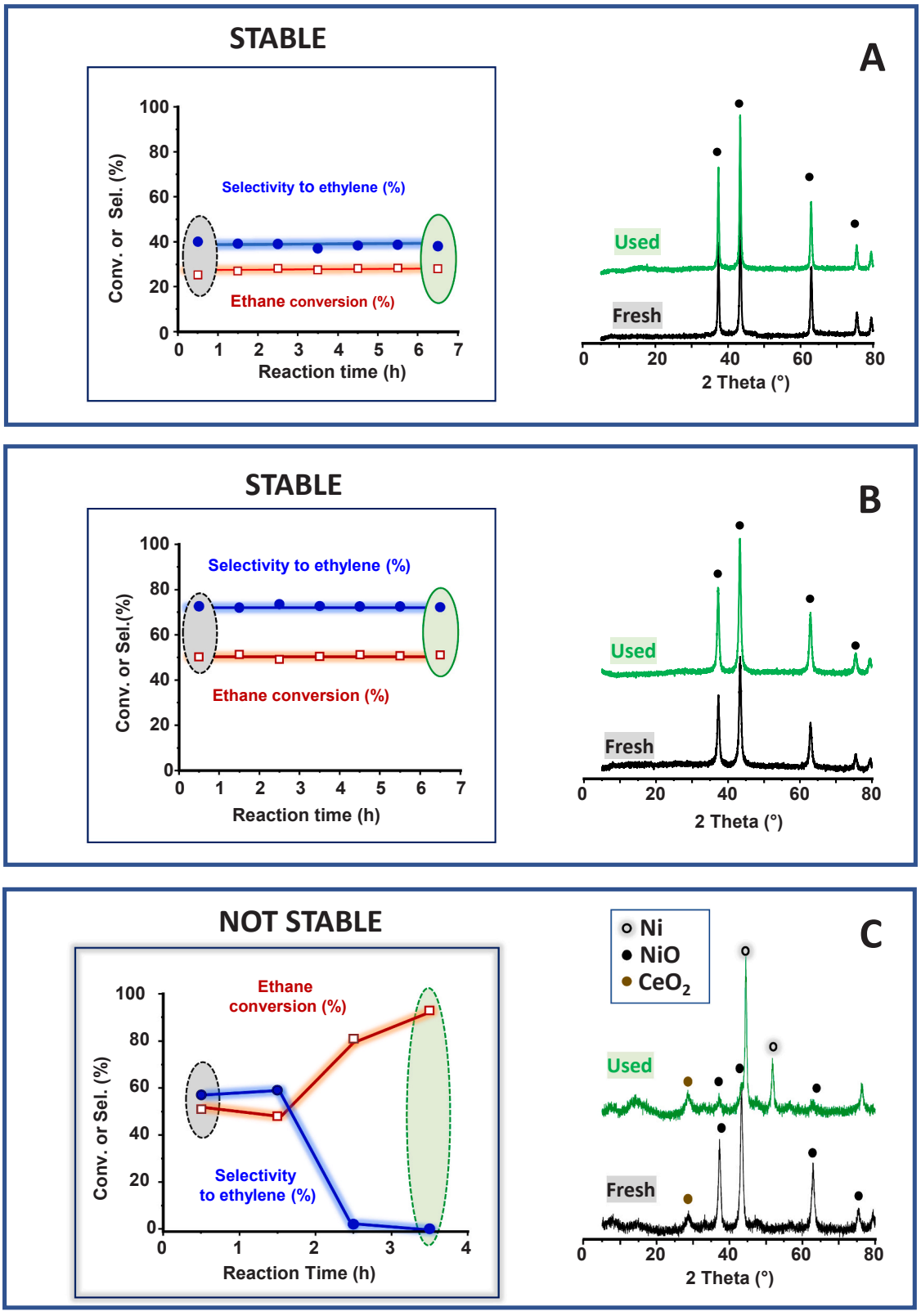

Fig. 5. Selectivity to ethylene (•) and ethane conversion (□) at a reaction temperature of 400 °C as a function of the reaction time in the N_2O assisted ODH of ethane (Left graphs). XRD pattern of catalysts both fresh and used after 7 h (Right graphs). Catalysts: **A)** NiO_{ref}; **B)** (Nb)NiO; **C)** (Ce)NiO. Reaction conditions in Experimental section.

powerful technique for analysing interfacial properties at electrode surfaces, for instance those on catalysts, i.e., it measures redox processes occurring at the electrode interface, including charge transfer resistance and the capacitance of the space charge layer [54–56]. It enables the investigation of mass transfer, charge transfer, and diffusion processes at the catalyst interface. Additionally, electrochemical processes related to redox reactions can be modelled using an equivalent circuit comprising electrical components such as resistances and constant phase elements. This equivalent circuit is designed to interpret and evaluate the individual components of the EIS system. From this model, the charge transfer resistance (linked to the active part of the catalyst that governs the kinetics of the redox-electrochemical reaction) can be calculated.

Nyquist (Fig. S4-A) and Bode-module (Fig. 6A and Fig. S4-B) plots have been undertaken for the different studied catalysts. The Nyquist plot displays the negative imaginary impedance (−Z'') against the real part of the impedance (Z'), while the Bode module plot presents the logarithm of the impedance modulus (|Z|) as a function of the logarithmic scale of the frequency. Through a careful study, which is explained in detail in Supporting Information, an evident correlation between the charge transfer resistance of the catalytic active parts of the samples (R_1 values) with the selectivity to ethylene has been observed. That is, the Nb-doped NiO catalyst, which presents the greatest selectivity to ethylene conversion in the ODH of ethane reaction activated with N_2O, shows the highest R_1 value, as opposed to the lowest charge

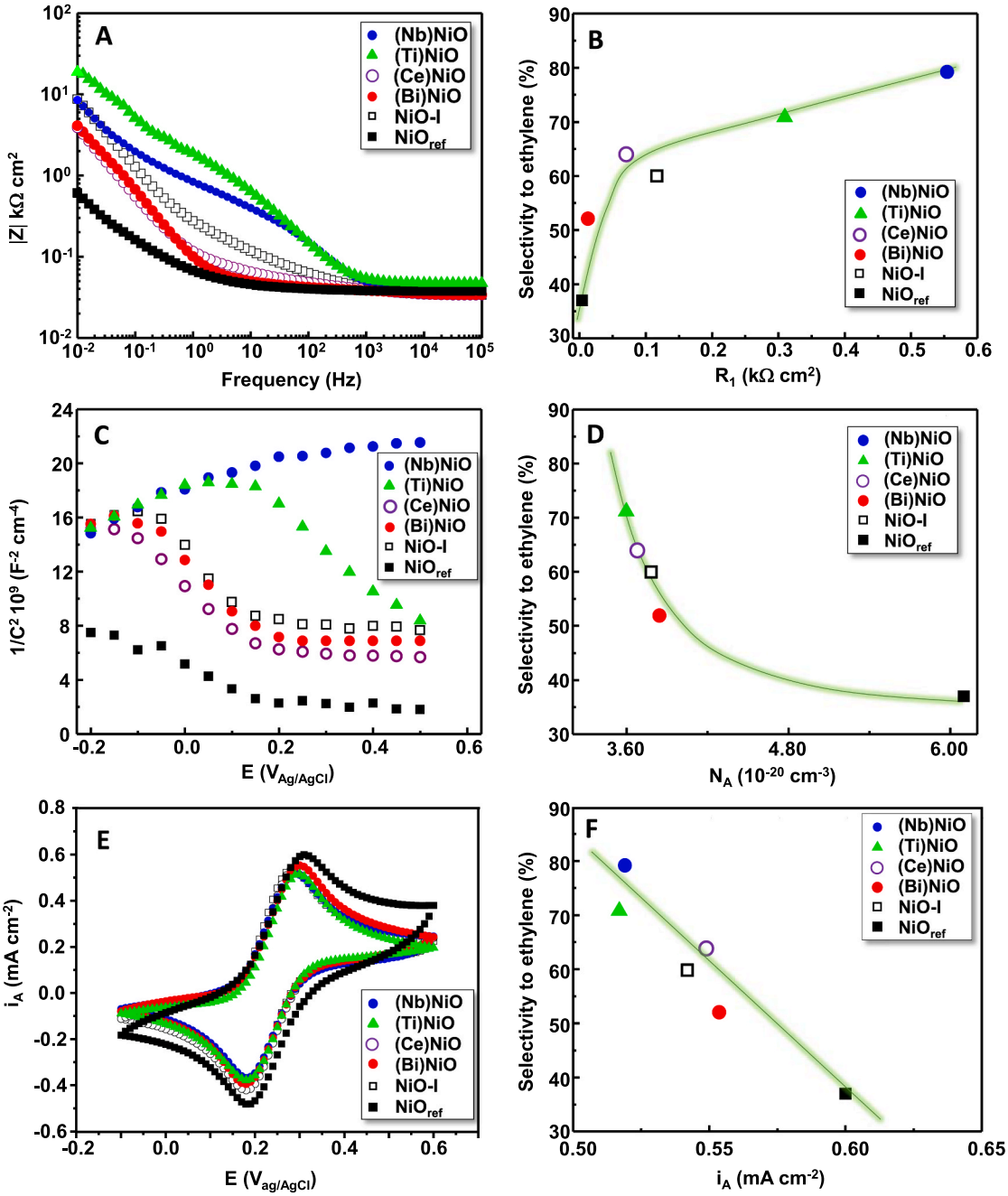

Fig. 6. Bode-module plots (**A**) and the corresponding relationship between the selectivity to ethylene during the ethane ODH assisted with N_2O and the charge transfer resistance of the active parts of the catalysts (R_1, charge-transfer resistance at the interfacial active sites of the catalysts) (**B**). Mott-Schottky plots (**C**) and the relationship between the selectivity to ethylene during the ethane ODH assisted with N_2O and density of acceptor defects, N_A (**D**). Cyclic voltammetries for the different NiO based catalysts (**E**), and the relationship between the selectivity to ethylene during the ethane ODH assisted with N_2O with the anodic current densities (**F**). Notes: Reaction conditions as in the text, 400 °C and 30 % ethane isoconversion.

transfer resistance values obtained for the NiO reference catalyst. According to this, the highest resistance values (related to the active surface of the catalysts), are more interesting from a catalytic point of view, since the selectivity to ethylene increases (Fig. 6B). We hypothesize that the total oxidation reactions should be somehow hindered or limited.

Through the representation of Mott-Schottky plots (Fig. 6C, and Fig. S5), specifically from the slope of the $1/C^2$ vs E plot (Eq. (1)), the type of conductivity as well as the density of acceptor defects, N_A, (corresponding to cationic vacancies in the space charge region or electrophilic non-selective oxygens in p-type semiconductors) can be estimated (see detailed info in Supporting Information). Thus, it was observed that all the samples present p-type semiconductivity with the exception of (Nb)NiO catalyst for which a positive slope can be elucidated. Moreover, regarding the catalysts with the p-type semiconductivity, the higher slopes are obtained for the samples with the greatest impedance resistances. N_A values were plotted vs selectivity to ethylene in the ODHE assisted with N_2O reaction (Fig. 6D), showing that the catalysts with higher N_A values (corresponding to a high number of electrophilic oxygen species) are the lower selective to ethylene towards ODHE with N_2O. More interesting to mention is the change in the semiconductive nature for the (Nb)NiO catalyst. For this sample, the compatible ion size of Nb^{5+} cations [30,32] might completely fill Ni^{2+} vacancies, thus hindering the p-type nature of the catalyst.

To complete the electrochemical characterization of the catalysts, cyclic voltammetries were carried out for 10 cycles (Fig. 6E, and Fig. S6) showing no significant differences between the first and the last cycle. For the studied catalysts an inverse correlation between anodic current densities and the selectivity to ethylene can be elucidated (Fig. 6F). We hypothesize that high electrochemical activity may favour total oxidation reactions, therefore decreasing the selectivity to the desired product. According to this, the best catalysts are the (Nb)NiO and (Ti)NiO which are also those presenting the highest impedance external resistances and the lowest N_A values.

In line with electrochemical results, the XPS data at the O 1s core line (Fig. 7 and Table S6) shows a higher contribution of non-stoichiometric low coordinated surface oxygen species (O^{2-}, O_2^{2-}, or O^-) with BE at 531.1 eV on both NiO_{ref} and NiO-I samples [57,58]. Both samples show the lowest selectivity to ethylene.

Furthermore, the contribution of these low coordinated oxygen species seem to be lower in the (Nb)NiO and (Ce)NiO samples, both of them with the highest selectivity to ethylene. However, and although these results underlie the critical role of surface oxygen species on the selectivity to ethylene, this is not the only variable that influences ethylene selectivity.

3.4. Temperature programmed reaction of N_2O and ethane/N_2O

Temperature programmed reaction experiments on representative catalysts for both the N_2O decomposition and the ethane ODH reaction assisted with N_2O are shown in Fig. 8 and Fig. 9, respectively.

In the case of N_2O decomposition (Fig. 8), small differences are observed among these catalysts, the activation of the N_2O taking place at low temperatures, i.e., below 300 °C, which indicates that the activation of N_2O occurs at lower temperatures than those required for ethane-ODH (Fig. 4).

Fig. 9 shows the TPR experiments for N_2O/ethane transformation over representative catalysts. In all cases, the onset of ethane consumption goes in parallel with N_2O consumption and N_2 formation, the activation temperature being similar to that found previously for N_2O decomposition in absence of alkane. In parallel to ethane consumption, ethene is clearly observed in all the cases, especially in (Nb)NiO catalyst (Fig. S7), this sample being the one that shows the highest ethylene yield in the catalytic studies. In addition, these experiments show a total consumption of N_2O on all the catalysts at temperatures lower than

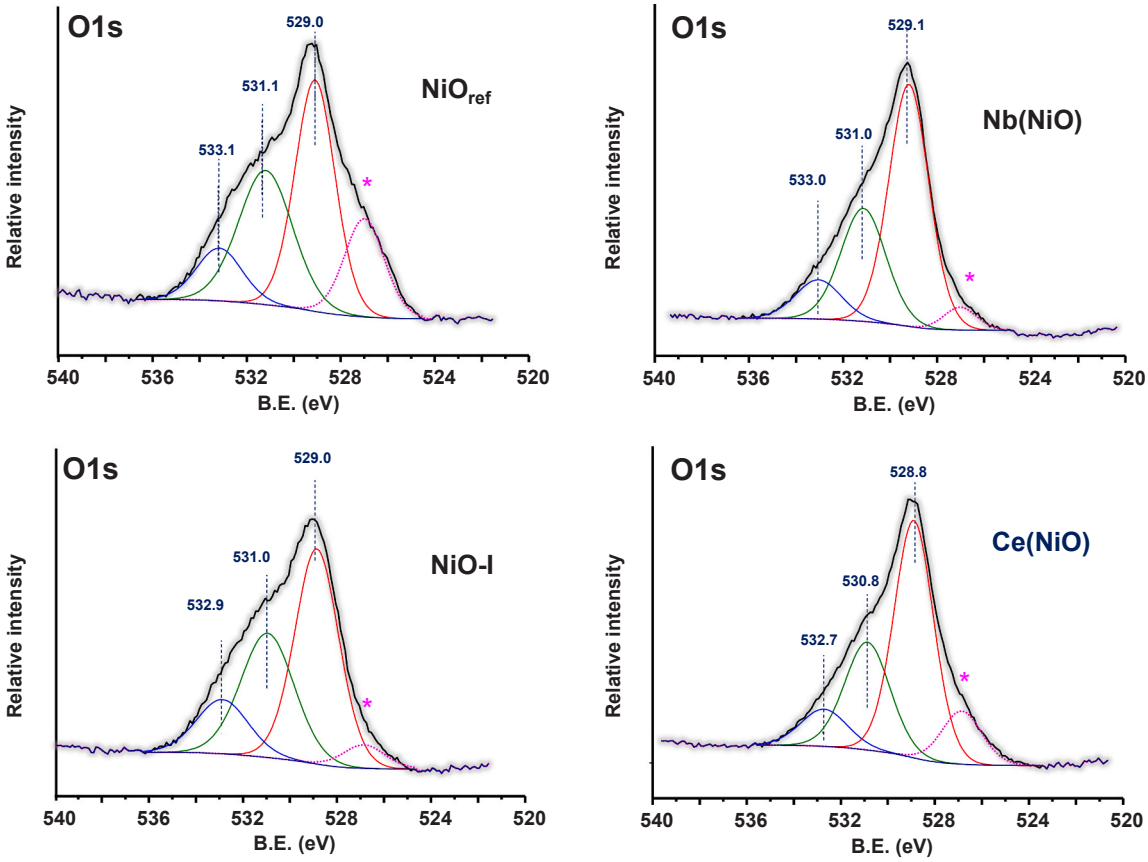

Fig. 7. The O1s XPS spectra of NiO based-catalysts. (*) Contribution of the sample holder.

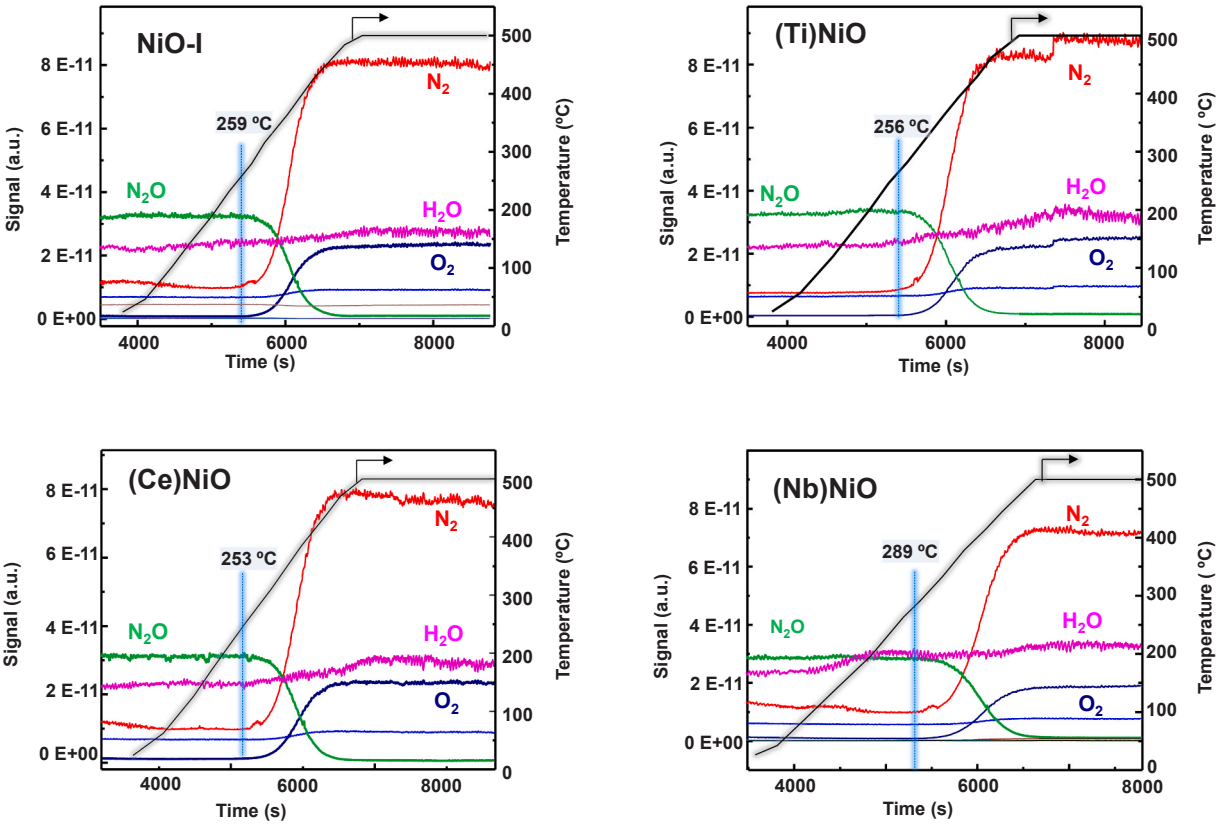

Fig. 8. TPR experiments for N_2O decomposition over representative catalysts: NiO-I; (Ti)NiO; (Ce)NiO; (Nb)NiO.

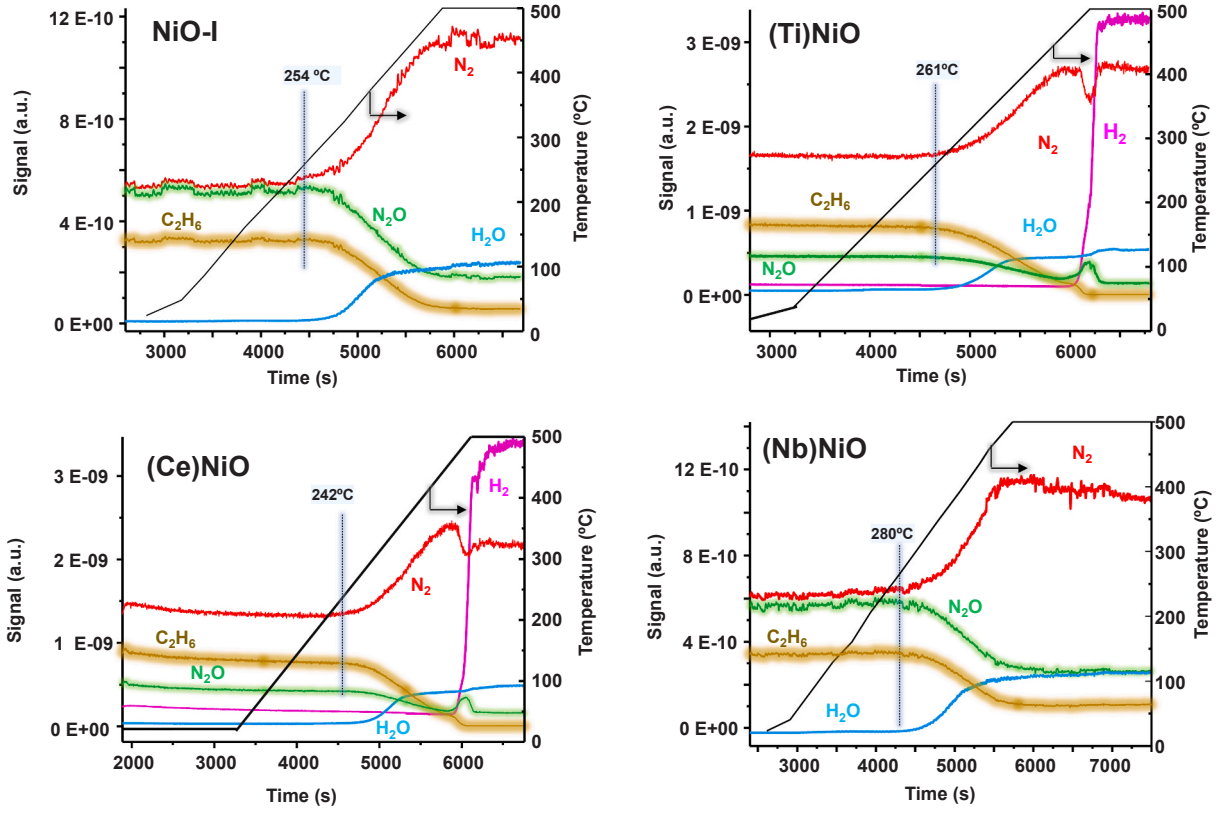

Fig. 9. TPR experiments for N_2O/ethane transformation over representative catalysts: NiO-I; (Ti)NiO; (Ce)NiO; (Nb)NiO.

500 °C. For the Ce^{4+}-containing NiO catalyst, hydrogen is formed when all the N_2O has been consumed, due to the reduction of the NiO into metallic Ni, which is in agreement with that observed in Fig. 4. Similarly, hydrogen production is also observed in the Ti-doped catalyst. Interestingly, hydrogen is not produced in the case of (Nb)NiO catalyst when all the nitrous oxide is consumed due to the non-reduction of the NiO phase. Thus, the use of Ce^{4+} as a promoter facilitates the reduction of NiO, unlike what happens with the Nb-promoted catalyst. This behaviour demonstrates the stability of the (Nb)NiO catalyst even at high temperatures (500 °C) and in the absence of oxidizing agent.

Accordingly, the TPR-N_2O and TPR-N_2O/ethane suggests that the activation of N_2O does not seem to be relevant in the different catalytic performance obtained by the distinct NiO-based catalysts during the N_2O-assisted ethane ODH, since the former reaction takes place at reaction temperatures (typically 400 °C) (Table 2) much higher than those of the N_2O decomposition (lower than 300 °C) (Figs. 8 and 9).

4. Discussion

In the present article, we have shown that promoted NiO catalysts are highly efficient for the N_2O-assisted ODH of ethane whenever the appropriate promoter is selected. It has been demonstrated that not all the promoters lead to an improved performance compared to an unpromoted NiO. Positively, the addition of Ce^{4+}, Ti^{4+} and, especially, Nb^{5+} enhances the selectivity to ethylene. With the optimal catalyst, (Nb)NiO, yields to ethylene of 40 % can be obtained in spite of the fact that the reaction conditions have not been optimized. Interestingly, this catalyst is highly stable, with the olefin formation being unchanged for at least 24 h. Moreover, this catalyst is very stable since the nickel oxide phase of (Nb)NiO is not reduced into metallic nickel even when the oxidizing agent (N_2O) has been exhausted during the reaction and then it can be re-used further with a negligible loss of performance. This excellent behaviour of (Nb)NiO catalyst contrasts with that of the other catalysts, (Ce)NiO and (Ti)NiO, which are also more selective than undoped **NiO-I**, but they develop into metallic nickel once they are in a N_2O-free atmosphere.

There exists in the oxygen assisted ODH of ethane a relationship between the valence of the promoter and the catalytic performance [24,29]. Thus, basic dopants (typically low valence elements) when incorporated into an oxide push the valence of the Ni to its highest accessible valence. However, acidic dopants (high valence state elements, such as Nb^{5+}) push the valence state of the host metal towards its lowest available valence. Then, non-stoichiometric nickel sites stabilize unselective electrophilic oxygen species and then lower ethylene formation is observed. Consequently, a correlation between the valence of the promoter and the selectivity to ethylene has been reported [24,29], in a way that the higher the valence of the cation promoter, the higher is the selectivity to the olefin. Accordingly, in the present article, the same general trend has been observed (Fig. S8). In the present article, a correlation between the XPS results and the catalytic results has not been observed, probably due to the difficult assignment of the nickel surface species.

As mentioned above (Fig. 7), the incorporation of high valence state cations into NiO decreases the number of electrophilic oxygens (O^-), i.e., the non-stoichiometric oxygen species associated with non-desired deep oxidation reactions [24,29,30,59–62]. These oxygen species are directly related to cationic vacancies, the main charge carriers in p-type catalysts [24,29,30,59–62]. Therefore, it has been demonstrated that using electrochemical techniques we can estimate the selectivity to ethylene of NiO based catalysts. This is in agreement to previous studies confirming that the most selective catalysts for ethane ODH are those with low concentration of electrophilic oxygen which can be properly assessed by electrochemical techniques [32], so that few cationic vacancies and low charge-transfer resistance at the interfacial active sites of the catalysts are positive properties for achieving high olefin selectivity.

In the O_2-assisted ODH of ethane on a Nb-NiO catalyst [60], by undertaking experiments with labelled oxygen, it was demonstrated that lattice oxygen participates in the selective oxidative dehydrogenation of ethane and also, to a lesser extent, in the total oxidation to CO_2. On the other hand, we have observed that the activation of N_2O on promoted and unpromoted NiO catalysts takes place at low reaction temperature (transforming into O_2 and N_2). Therefore, we propose a mechanism for the N_2O-assisted ODH of ethane similar that that for O_2-assisted ODH of ethane but with a previous step for the N_2O activation, which according to our results (high activity for all catalysts for N_2O decomposition at relatively low temperature) is not the rate-limiting step. In any case, we want to remark that this is not a mechanistic study and a more detailed study could provide more insights into the real mechanism of this reaction.

Additional experiments have been performed with low ethane conversions and changing the ethane to N_2O ratio in order to estimate the reaction orders. According to our new experiments, the formation of ethylene presents a reaction order with respect to ethane of 0.52 and 0.25 with respect to N_2O. The formation of CO_2 presents a reaction order with respect to ethane of 0.61 and 0.72 with respect to N_2O. These values are similar to those reported in ref. [60] with a Nb-doped NiO catalyst in the O_2-assisted ODH of ethane in which the reaction orders with respect to ethane and O_2 for the formation of ethylene were 0.55 and 0.83, respectively. In the same way, the formation of CO_2 for N_2O-assisted ethane ODH presented reaction orders similar to those proposed for the formation of CO_2 during the O_2-assisted ethane ODH to ethane (0.55 and 0.83 with respect to ethane and O_2 respectively). Accordingly, a similar reaction mechanism than that proposed for O_2-assisted ethane ODH [30,60–62] can be suggested for N_2O-assisted ethane ODH, with an initial step for the N_2O decomposition, which is very fast and cannot be considered as the rate limiting step, and in which lattice oxygen is directly involved in the ethane ODH, while the incorporation of O_2 [60,62] or N_2O can be mainly related with the reoxidation of the catalysts.

Due to the redox mechanism of the overall N_2O-assisted ODH of ethane, the study of the reducibility of nickel oxide-based catalysts could help to explain the catalytic behaviour observed, especially considering that the reduction is usually the limiting step in the O_2-ODH [30,32] at high and moderate reaction temperatures.

Unfortunately, no relationship can be established between the catalytic activity (either per mass or per area of catalyst) and the reducibility of the catalyst, considering either the temperature for maximum hydrogen consumption (TPR_{max}) or the onset temperature in the TPR experiments (T_{onset}) (Fig. S9).

We must indicate that, in some cases during the O_2-ODH of ethane, the highly reducible sites are often related to unselective electrophilic oxygen sites and then, the most selective active sites are those that present the lowest reducibility [28,63]. Nevertheless, in the present study no relationship has been observed between the selectivity to the olefin and the reducibility of the catalysts (Fig. S9, supplementary information). Maybe the different nature of the dopants employed can be one of the reasons for that lack of trend as well as the fact that the reduction in the TPR experiments has been conducted using hydrogen, which is not present in the reaction mixture in the ODH reaction. Thus, additional temperature programmed reactions with N_2O or with ethane/N_2O have been undertaken.

On the other hand, the comparison between the ODH of ethane using nitrous oxide and molecular oxygen with the Nb^{5+}-promoted NiO catalyst indicates that the selectivity to ethylene (fixing the reaction temperature and the alkane conversion) using N_2O is ca. 8 points higher than when O_2 is used (Table S4). Moreover, unlike the other catalytic systems reported in the literature such as VO_x/MCM41 [6] or MoO_x/SiO_2-TiO_2 [9], the reaction rates are pretty similar regardless of the oxidizing agent used (O_2 or N_2O). For example, in the case of the VO_x/MCM41 catalysts the reaction rate was 5–6 times larger using O_2 than with N_2O [6]. This different behaviour observed in Ni-containing catalysts respect to that observed in V-containing catalysts is related to the

relatively high activity of NiO-based catalysts for N_2O decomposition, in which small differences for undoped and doped catalyst can be proposed from TPR-N_2O (Fig. 8) and TPR-N_2O/Ethane (Fig. 9) experiments. In other words, a high reoxidation rate of catalysts can be proposed for undoped and doped NiO-containing catalysts, with active oxygen species on the catalysts surface, which can take place at temperatures much lower than those that the N_2O-ODH of ethane have been carried out in the present study. This is likely the reason for the similar reactivity observed with N_2O and O_2.

Otto and Shelef [13] studied the exchange of oxygen on the surface of NiO with $N_2^{18}O$. It was observed that at 400 °C the oxygen exchange between NiO and N_2O takes place suggesting the generation of a surface complex although this exchange is very slow. Conversely, most of N_2O was readily decomposed into N_2 and O_2. These results are in agreement with the high reactivity observed in the present article in the N_2O decomposition even at low temperatures. On the other hand, the mechanism of the ODH of ethane using molecular oxygen on NiO and Nb-promoted NiO catalysts has been proposed [30]. According to that article, the cleavage of the C—H bond is the determining step whereas the rate determining step for the ethylene oxidation is the C═C bond cleavage. Interestingly, the activation of ethane over the catalytic surface involves the substraction of a hydrogen atom by O^- species, with the formation of an alkyl radical. The "site isolation" principle proposes that active oxygen (or, in general, active sites) must be isolated to prevent decomposition or overoxidation of the desired dehydrogenated or partially oxidized product [64,65]. Thus, by the isolated sites principle, low electrophilic oxygen concentration leads to the olefin formation with high selectivity whereas high concentrations lead to the oxidation to CO_2 of the ethyl radicals previously formed. Therefore, it is paramount the control of the relative coverage of surface O species and their redox state on the surface.

According to the results obtained in the present work, probably N_2O decomposes into N_2 and O_2, and then the same sequence reported takes place (firstly the alkyl radical is formed and then the dehydrogenation or the total oxidation occurs on the catalyst surface with low or high concentration of O^- sites). Accordingly, a redox parallel-consecutive reaction network with the participation of two types of active sites, as suggested for O_2-assisted ethane ODH [30,60–62], can be proposed in the case of Nb-doped NiO catalyst: **Nb**—O—Ni—O pairs responsible for the ethane ODH and ethene overoxidation reaction; and Ni—O—Ni—O pairs, active for the direct oxidation of ethane to CO_2. In the case of other promoters, the selectivity to ethylene can be explained as considering the [**Me**—O—Ni—O pairs]/[Ni—O—Ni—O pairs] ratio, although in some cases a direct participation of the Me-O promoter cannot be completely ruled out.

Among the different promoted NiO catalysts, the catalytic performance for ethane N_2O-assisted ODH is related to the nature of surface sites (electrophilic O^- sites) and its concentration, as previously suggested for O_2-assisted ethane ODH [29,30,60–62], which is strongly influenced by the valence and the acid/base characteristics of the metal oxide promoters, with a great impact on the selectivity to ethylene. On the other hand, the redox cycle should be concluded after the catalyst reoxidation. In the case of O_2-assisted reaction via the interaction of gas phase oxygen with formed anionic vacancies [30]. In the case of N_2O-assisted reaction for NiO-based catalyst, the N_2O decomposition is very fast (Fig. 8). Accordingly, the reoxidation of catalysts with N_2O should be similar to that proposed for O_2.

Another aspect that could have an influence on the catalytic behavior of these catalysts is the porosity. For the NiO based catalysts the microporosity is nearly absent so that its role in the catalytic performance of porosity is negligible. This contrasts with the behavior of multicomponent M1 catalysts in which their heptagonal channel micropores seems to host highly selective sites for ethane activation [66,67].

We have also studied the effect of co-feeding water or CO_2 on the most selective catalyst (Nb)NiO (Fig. S10). Interestingly, the presence of water has meant a slight decrease of the conversion (from ca. 31 to 27 %) and a slight increase of the selectivity to the olefin (from ca. 77 to 81 %). The addition of very low concentrations of CO_2 has not modified the results compared to the standard reaction conditions. In all cases, the catalytic performance was stable with the reaction time.

The enhanced selectivity observed using Nb-doped NiO with N_2O compared to O_2 is significant and is not straightforward to explain. We propose the following:

i) at isoconversion conditions, the selectivity to ethylene decreases when the concentration of O_2 increases (Fig. S11).
ii) on the other hand, if N_2O is used as an oxidant, two reactions will take place rather simultaneously, the transformation of N_2O into oxygen plus the ODH of ethane.
iii) in the upper part of the catalyst bed the concentration of active O-atoms will be lower when feeding N_2O, since only a portion of N_2O will have been transformed into O_2 and therefore, the selectivity to ethylene will be higher.

Other factors such as a possible lower oxidation state of nickel sites on the surface during reaction with nitrous oxide than with molecular oxygen or changes in the nature of oxygen species cannot be ruled out (Fig. 7) [6,9].

Overall, we have observed that the N_2O assisted ODH of ethane is technically better than that with oxygen, increasing the selectivity to ethylene while maintaining the catalytic activity. It is true that from an environmental viewpoint it is not so clear that the N_2O emissions would decrease, although the use of this process in facilities where N_2O is produced in high concentrations would be very useful. Aside from that, this technology presents several challenges, as it requires the co-location of point sources of N_2O emissions with hydrocarbon feedstocks and the recovery of ethylene from these streams.

5. Conclusions

Unpromoted and promoted NiO catalysts can be very efficient in the N_2O-assisted oxidative dehydrogenation of ethane, whenever the synthesis conditions and the nature of the promoter are controlled.

The catalytic results for N_2O-assisted ethane ODH over NiO-based catalysts show higher selectivity to ethylene than when the reaction is carried out in the presence of oxygen. All catalysts show a high effectiveness in the decomposition of N_2O, which guarantees a fast reoxidation rate of the catalyst during the catalytic tests. The differences in the catalytic results for N_2O-assisted ODH are related to the changes produced in the catalyst as a consequence of the presence of different promoters. This behaviour is completely different from that observed in vanadium-containing catalysts, in which the catalytic properties are related to a low reoxidation rate in the presence of N_2O.

In our case, the best option is to use Nb^{5+} as a promoter. In fact, Nb-doped NiO catalyst probably presents the best catalytic performance reported in the literature in terms of catalytic activity, selectivity to the olefin and robustness. Ethylene yields of 40 % have been achieved.

On the other hand, no correlation has been found between the ethylene formation and the results obtained by TPR-H_2 (reducibility) or by XPS (characteristics of nickel species on the near surface). However, the selectivity to ethylene observed presents a close link with the electrochemical properties of the catalysts. Thus, the most selective catalysts are those with lower density of acceptor defects (cationic vacancies) and higher charge-transfer resistance at the interfacial active sites of the catalysts. As a general trend, those catalysts with less oxidized surface tend to be more selective towards the formation of ethylene as it has been also proposed for O_2-asisted ethane ODH.

CRediT authorship contribution statement

G. Sánchez-García: Validation, Investigation. **A. Pérez-Calvo:**

Validation, Investigation. **B. Moreno-Torralbo:** Investigation. **R. Sánchez-Tovar:** Validation, Methodology, Funding acquisition. **A.M. Dejoz:** Methodology, Investigation, Funding acquisition. **P. Concepción:** Investigation, Funding acquisition. **J.M. López Nieto:** Supervision, Funding acquisition, Conceptualization. **B. Solsona:** Writing – review & editing, Supervision, Funding acquisition, Conceptualization.

Declaration of competing interest

The authors declare that they have no known competing financial interests or personal relationships that could have appeared to influence the work reported in this paper.

Acknowledgements

The funding received for this study from the Spanish Ministry of Science and Innovation, projects PID2021–126235OB-C31 and PID2021–126235OB-C33 (funded by MCIN/ AEI/10.13039/501100011033 and FEDER funds) and projects TED2021–130756B-C31 and TED2021-129555B-I00 (funded by MCIN/AEI/10.13039/501100011033 and by "ERDF A way of making Europe" by the European Union NextGenerationEU/PRTR), is acknowledged. BMT, PC, and JMLN also thank CEX2021-001230-S grant funded by MCIN/AEI/10.13039/501100011033. G. Sánchez-García is also grateful to the Generalitat Valenciana (CIACIF/2021/010) and A. Pérez-Calvo to Ministerio de Ciencia, Innovación y Universidades (FPU23/02557).

Appendix A. Supplementary data

Supplementary data to this article can be found online at https://doi.org/10.1016/j.jcat.2025.116277.

Data availability

Data will be made available on request.

References

[1] EPA, United States Environmental Protection Agency, Overview of Greenhouse gases. https://www.epa.gov/ghgemissions/overview-greenhouse-gases, 2024 (accessed 11 April 2024).
[2] IPCC, 2021: Climate Change 2021: The Physical Science Basis. Contribution of Working Group I to the Sixth Assessment Report of the Intergovernmental Panel on Climate Change, in: V. Masson-Delmotte, P. Zhai, A. Pirani, S.L. Connors, C. Péan, S. Berger, N. Caud, Y. Chen, L. Goldfarb, M.I. Gomis, M. Huang, K. Leitzell, E. Lonnoy, J.B.R. Matthews, T.K. Maycock, T. Waterfield, O. Yelekçi, R. Yu, B. Zhou (Eds.), Cambridge University Press, Cambridge, United Kingdom and New York, 2021. doi:10.1017/9781009157896.
[3] H. Tian, R. Xu, J.G. Canadell, et al., A comprehensive quantification of global nitrous oxide sources and sinks, Nature 586 (2020) 248–256.
[4] S. He, Y. Han, X. Qin, Advances in accounting methodology of nitrous oxide emissions from the adipic acid industry, J. Environ. Sci. (2024), https://doi.org/10.1016/j.jes.2024.03.014 (in press).
[5] J.H. Carter, T. Bere, J.R. Pitchers, D.G. Hewes, B.D. Vandegehuchte, C.J. Kiely, S. H. Taylor, G.J. Hutchings, Direct and oxidative dehydrogenation of propane: from catalyst design to industrial application, Green Chem. 23 (2021) 9747–9799.
[6] O. Ovsitser, E.V. Kondratenko, Similarity and differences in the oxidative dehydrogenation of C_2–C_4 alkanes over nano-sized VO_x species using N_2O and O_2, Catal. Today 142 (2009) 138–142.
[7] E.V. Kondratenko, A. Brückner, On the nature and reactivity of active oxygen species formed from O_2 and N_2O on VO_x/MCM-41 used for oxidative dehydrogenation of propane, J. Catal. 274 (2010) 111–116.
[8] X. Rozanska, E.V. Kondratenko, J. Sauer, Oxidative dehydrogenation of propane: differences between N_2O and O_2 in the reoxidation of reduced vanadia sites and consequences for selectivity, J. Catal. 256 (2008) 84–94.
[9] M.P. Woods, B. Mirkelamoglu, U.S. Ozkan, Oxygen and nitrous oxide as oxidants: implications for ethane oxidative dehydrogenation over silica−titania-supported molybdenum, J. Phys. Chem C. 113 (2009) 10112–10119.
[10] M.B. Ward, M.J. Lin, J.H. Lunsford, The oxidative dehydrogenation of ethane by nitrous oxide over molybdenum oxide supported on silica gel, J. Catal. 50 (1977) 306–318.
[11] A.S. Kharitonov, G.I. Panov, G.A. Sheveleva, L.V. Pirutko, T.P. Voskresenskaya, V.I. Sobolev, Catalysts for production of phenol and its derivatives. US Patent 5,672,777 (1997); assigned to Monsanto Co.
[12] A. Held, J. Kowalska, K. Nowińska, Nitrous oxide as an oxidant for ethane oxydehydrogenation, Appl. Catal. B- Environm. 64 (2006) 201–208.
[13] K. Otto, M. Shelef, Studies of surface reactions of NO by isotope labeling: VII. Oxygen exchange between nickel oxide and $N^{18}O$, $^{18}O_2$ and $N_2^{18}O$, J. Catal. 35 (1974) 460–471.
[14] P. Botella, A. Dejoz, M.C. Abello, M.I. Vázquez, L. Arrua, J.M. López Nieto, Selective oxidation of ethane: developing an orthorhombic phase in Mo–V–X (X = Nb, Sb, Te) mixed oxides, Catal. Today 142 (2009) 272–277.
[15] D. Melzer, G. Mestl, K. Wanninger, Yu. Zhu, N.D. Browning, M. Sanchez-Sanchez, J.A. Lercher, Design and synthesis of highly active MoVTeNb-oxides for ethane oxidative dehydrogenation, Nat. Commun. 10 (2019) 4012.
[16] A. de Arriba, G. Sánchez, R. Sánchez-Tovar, P. Concepción, R. Fernández-Domene, B. Solsona, J.M. López Nieto, On the selectivity to ethylene during ethane ODH over M1-based catalysts. a surface and electrochemical study, Catal. Today 418 (2023) 114122.
[17] P.J. Donaubauer, D.M. Melzer, K. Wanninger, G. Mestl, M. Sanchez-Sanchez, J. A. Lercher, O. Hinrichsen, Intrinsic kinetic model for oxidative dehydrogenation of ethane over MoVTeNb mixed metal oxides: a mechanistic approach, Chem. Eng. J. 383 (2020) 1231959.
[18] T. Konya, T. Katou, T. Murayama, S. Ishikawa, M. Sadakane, D. Buttrey, W. Ueda, An orthorhombic Mo_3VOx catalyst most active for oxidative dehydrogenation of ethane among related complex metal oxides, Catal. Sci. Technol. 3 (2013) 380–387.
[19] E. Heracleous, A.A. Lemonidou, Ni–Nb–O mixed oxides as highly active and selective catalysts for ethene production via ethane oxidative dehydrogenation. Part I: characterization and catalytic performance, J. Catal. 237 (2006) 162–174.
[20] P. Brussino, E.L. Mehring, M.A. Ulla, J.P. Bortolozzi, Tuning the properties of NiO supported on silicon-aluminum oxides: influence of the silica amount in the ODH of ethane, Catal. Today 394–396 (2022) 133–142.
[21] D. Delgado, B. Solsona, R. Sanchis, E. Rodríguez-Castellón, J.M. López Nieto, Oxidative dehydrogenation of ethane on diluted or promoted nickel oxide catalysts: influence of the promoter/diluter, Catal. Today 363 (2021) 27–35.
[22] R. Sanchis, D. Delgado, S. Agouram, M.D. Soriano, M.I. Vázquez, E. Rodríguez-Castellón, B. Solsona, J.M. López Nieto, NiO diluted in high surface area TiO_2 as an efficient catalyst for the oxidative dehydrogenation of ethane, Appl. Catal. A- Gen. 536 (2017) 18–26.
[23] Y. Abdelbaki, A. de Arriba, B. Solsona, D. Delgado, E. García-González, R. Issaadi, J.M. López Nieto, The nickel-support interaction as determining factor of the selectivity to ethylene in the oxidative dehydrogenation of ethane over nickel oxide/alumina catalysts, Appl. Catal. A-Gen. 623 (2021,) 118242.
[24] E. Heracleous, A.A. Lemonidou, Ni–Me–O mixed metal oxides for the effective oxidative dehydrogenation of ethane to ethylene – effect of promoting metal Me, J. Catal. 270 (2010) 67–75.
[25] B. Savova, S. Loridant, D. Filkova, J.M.M. Millet, Ni–Nb–O catalysts for ethane oxidative dehydrogenation, Appl. Catal. A-Gen. 390 (2010) 148–157.
[26] H. Zhu, S. Ould-Chikh, D.H. Anjum, M. Sun, G. Biuasque, J.-M. Basset, B. Caps, Nb effect in the nickel oxide catalyzed low-temperature oxidative dehydrogenation of ethane, J. Catal. 285 (2012) 292–303.
[27] B. Solsona, P. Concepcion, B. Demicol, S. Hernández, J.J. Delgado, J.J. Calvino, J. M. López Nieto, Selective oxidative dehydrogenation of ethane over SnO_2-promoted NiO catalysts, J. Catal. 295 (2012) 104–114.
[28] H. Zhu, D.C. Rosenfeld, M. Harb, D.H. Anjum, M.N. Hedhili, S. Ould-Chikh, J.-M. Basset, Ni–M–O (M = Sn, Ti, W) catalysts prepared by a dry mixing method for oxidative dehydrogenation of ethane, ACS Catal. 6 (2016) 2852–2866.
[29] J.M. López Nieto, B. Solsona, R.K. Grasselli, P. Concepcion, Promoted NiO catalysts for the oxidative dehydrogenation of ethane, Top. Catal. 57 (2014) 1248–1255.
[30] Z. Skoufa, E. Heracleous, A.A. Lemonidou, On ethane ODH mechanism and nature of active sites over NiO-based catalysts via isotopic labelling and methanol sorption studies, J. Catal. 322 (2015) 118–129.
[31] D. Delgado, B. Solsona, A. Ykrelef, A. Rodríguez-Gómez, A. Caballero, E. Rodríguez-Aguado, E. Rodríguez-Castellón, J.M. López Nieto, Redox and catalytic properties of promoted NiO catalysts for the oxidative dehydrogenation of ethane, J. Phys. Chem. C 121 (2017) 25132–25142.
[32] Y. Abdelbaki, R. Sánchez-Tovar, A. de Arriba, E. García-González, R. Fernández-Domene, B. Solsona, J.M. López Nieto, Predicting the catalytic performance of Nb-doped nickel oxide catalysts for the oxidative dehydrogenation of ethane by knowing their electrochemical properties, J. Catal. 420 (2023) 9–22.
[33] Y.F.Y. Yao, J.T. Kummer, The oxidation of hydrocarbons and CO over metal oxides, I. NiO crystals, J. Catal. 28 (1973) 124–138.
[34] Y. Abdelbaki, A. de Arriba, R. Issaadi, R. Sanchez-Tovar, B. Solsona, J.M. López Nieto, Optimization of the performance of bulk NiO catalyst in the oxidative dehydrogenation of ethane by tuning the synthesis parameters, Fuel Process. Technol. 229 (2022) 107182.
[35] D. Delgado, R. Sanchis, B. Solsona, P. Concepción, J.M. López Nieto, Influence of the nature of the promoter in NiO catalysts on the selectivity to olefin during the oxidative dehydrogenation of propane and ethane, Top. Catal. 63 (2020) 1731–1742.
[36] M. Konsolakis, Recent advances on nitrous oxide (N_2O) decomposition over non-Noble-metal oxide catalysts: catalytic performance, mechanistic considerations, and surface chemistry aspects, ACS Catal. 5 (2015) 6397–6421.
[37] M. Xu, H.-X. Wang, H.-D. Ouyang, L. Zhao, Q. Lu, Direct catalytic decomposition of N_2O over bismuth modified NiO catalysts, J. Hazard. Mater. 401 (2021) 123334.
[38] F. Zhang, X. Wang, X. Zhang, M. Turxun, H. Yu, J. Zhao, The catalytic activity of NiO for N_2O decomposition doubly promoted by barium and cerium, Chem. Eng. J. 256 (2014) 365–371.

[39] N. Pasha, N. Lingaiah, P. Siva Sankar Reddy, P.S. Sai Prasad, An investigation into the effect of Cs promotion on the catalytic activity of NiO in the direct decomposition of N_2O, Catal. Lett. 118 (2007) 64–68.
[40] H. Zhou, P. Hu, Zh. Huang, F. Qin, W. Shen, H. Xu, Preparation of NiCe mixed oxides for catalytic decomposition of N_2O, Ind. Eng. Chem. Res. 52 (2013) 4504–4509.
[41] F. Zhao, Ch. Wang, D. Wang, Y. Yin, J. Yu, J. Han, J. Zeng, H. Chang, Efficient catalytic decomposition of N_2O over Cd-doped NiO in the presence of O_2, Appl. Catal. A-Gen. 649 (2023) 118946.
[42] Y. Zhou, J. Lin, L. Li, M. Tian, X. Li, X. Pan, Y. Chen, X. Wang, Improving the selectivity of Ni-Al mixed oxides with isolated oxygen species for oxidative dehydrogenation of ethane with nitrous oxide, J. Catal. 377 (2019) 438–448.
[43] Y. Zhou, F. Wei, J. Lin, L. Li, X. Li, H. Qi, X. Pan, X. Liu, Ch. Huang, S. Lin, X. Wang, Sulfate-modified NiAl mixed oxides as effective C−H bond-breaking agents for the sole production of ethylene from ethane, ACS Catal. 10 (2020) 7619–7629.
[44] G. Sánchez, A.M. Dejoz, R. Fernandez-Domene, I. Barroso Martin, D. Balesteros-Plata, A. Infantes-Molina, J.A. Cecilia, E. Rodrígez-Castellón, J.M. López Nieto, R. Sánchez-Tovar, B. Solsona, N_2O assisted ethane transformation into ethylene using NiO-CeO_2-ZrO_2 catalysts, ChemCatChem (2024) e202400329.
[45] X. Xu, S.K. Megarajan, X. Xia, A. Toghan, A. Feldhoff, Y. Zhang, H. Jiang, Effect of reduction temperature on the structure and catalytic performance of mesoporous Ni–Fe–Al2O3 in oxidative dehydrogenation of ethane, New J. Chem. 44 (2020) 18994–19001.
[46] I. Popescu, E. Heracleous, Z. Skoufa, A.A. Lemonidou, L.-C. Marcu, Study by electrical conductivity measurements of semiconductive and redox properties of M-doped NiO (M = Li, Mg, Al, Ga, Ti, Nb) catalysts for the oxidative dehydrogenation of ethane, Phys. Chem. Chem. Phys. 16 (2014) 4962–4970.
[47] F. Medina, P. Salagre, J.L.G. Fierro, J.E. Sueiras, NiO reducibilities: structural and catalytic properties of their pure and potassium-doped reduced forms, J. Catal. 142 (1993) 392–405.
[48] B. Solsona, J.M. López Nieto, P. Concepción, A. Dejoz, F. Ivars, M.I. Vázquez, Oxidative dehydrogenation of ethane over Ni–W–O mixed metal oxide catalysts, J. Catal. 280 (2011) 28–39.
[49] J.C. Vedrine, G. Hollinger, T.M. Duc, Investigations of antigorite and nickel supported catalysts by X-ray photoelectron spectroscopy, J. Phys. Chem. 82 (1978) 1515–1520.
[50] M.A. van Veenendaal, G.A. Sawatzky, Nonlocal screening effects in 2p x-ray photoemission spectroscopy core-level line shapes of transition metal compounds, Phys. Rev. Lett. 70 (1993) 2459–2462.
[51] V. Biju, M.A. Khadar, Electronic structure of nanostructured nickel oxide using Ni 2p XPS analysis, J. Nanopart. Res. 4 (2002) 247–253.
[52] K.I. Hadjiivanov, G.N. Vayssilov, Characterization of oxide surfaces and zeolites by carbon monoxide as an IR probe molecule, Adv. Catal. 47 (2002) 307–511.
[53] V. Bolis, G. Cerrato, G. Magnacca, C. Morterra, Surface acidity of metal oxides. Combined microcalorimetric and IR-spectroscopic studies of variously dehydrated systems, Thermoch. Acta 312 (1998) 63–77.
[54] A.C. Lazanas, M.I. Prodromidis, Electrochemical impedance spectroscopy—a tutorial, ACS Meas. Sci. Au 3 (2023) 162–193.
[55] H.S. Magar, R.Y.A. Hassan, A. Mulchandani, Electrochemical Impedance Spectroscopy (EIS): principles, Construction, and Biosensing Applications 21 (2021) 6578.
[56] T. Pajkossy, R. Jurczakowski, Electrochemical impedance spectroscopy in interfacial studies, Curr. Opin. Electrochem. 1 (2017) 53–58.
[57] J.-C. Dupin, D. Gonbeau, Ph. Vinatier, A. Levasseur, Systematic XPS studies of metal oxides, hydroxides and peroxides, Phys. Chem. Chem. Phys. 2 (2000) 1319–1324.
[58] X. Wen, K. Xie, Regulating lattice oxygen on the surfaces of porous single-crystalline NiO for stabilized and enhanced CO oxidation, Catalysts 14 (2024) 130.
[59] A. Ykrelef, L. Nadji, R. Issaadi, S. Agouram, E. Rodríguez-Castellón, B. Solsona, J. M. López Nieto, Mixed oxide Ti-Si-O prepared by non-hydrolytic xerogel method as a diluter of nickel oxide for the oxidative dehydrogenation of ethane, Catal. Today 299 (2018) 93–101.
[60] E. Heracleous, A.A. Lemonidou, Ni–Nb–O mixed oxides as highly active and selective catalysts for ethene production via ethane oxidative dehydrogenation. Part II: mechanistic aspects and kinetic modeling, J. Catal. 237 (2006) 175–189.
[61] E. Moreno-Barrueta, C. Alvarado-Camacho, J.F. Durán-Pérez, A.A. Morales-Pérez, C.O. Castillo, On the dynamics of the catalytic surface of a bimetallic mixed-oxide formulation during the oxidative dehydrogenation of ethane, Catal. Today 394–396 (2022) 161–177.
[62] C. Alvarado-Camacho, J. Poissonnier, J.W. Thybaut, C.O. Castillo, Unravelling the redox mechanism and kinetics of a highly active and selective Ni-based material for the oxidative dehydrogenation of ethane, React Chem. Eng. 7 (2022) 619–640.
[63] L. Kong, D. Li, Z. Zhao, J. Li, L. Zhao, X. Fan, X. Xiao, Z. Xie, Preparation, characterization and catalytic performance of rod-like Ni–Nb–O catalysts for the oxidative dehydrogenation of ethane at low temperature, Catal. Sci. Technol. 9 (2019) 3416–3442.
[64] R.K. Grasselli, Advances and future trends in selective oxidation and ammoxidation catalysis, Catal. Today 49 (1999) 141–153.
[65] R.K. Grasselli, Selectivity issues in (amm)oxidation catalysis, Catal. Today 99 (2005) 23–31.
[66] L. Annamalai, Y. Liu, S. Ezenwa, Y. Dang, S.L. Suib, P. Deshlahra, Influence of tight confinement on selective oxidative dehydrogenation of ethane on MoVTeNb mixed oxides, ACS Catal. 8 (2018) 7051–7067.
[67] S. Ishikawa, X. Yi, T. Murayama, W. Ueda, Heptagonal channel micropore of orthorhombic Mo_3VO_x as catalysis field for the selective oxidation of ethane, Catal. A: Gen. 474 (2014) 10–17.